

RESEARCH ARTICLE

Competitive Mirror Image Phage Display Derived Peptide Modulates Amyloid Beta Aggregation and Toxicity

Stephan Rudolph¹, Antonia Nicole Klein¹, Markus Tusche¹, Christine Schlosser¹, Anne Elfgen¹, Oleksandr Brener^{1,3}, Charlotte Teunissen⁴, Lothar Gremer^{1,3}, Susanne Aileen Funke^{1,2}, Janine Kutzsche¹, Dieter Willbold^{1,3*}

1 Institute of Complex Systems, Structural Biochemistry (ICS-6), Research Centre Jülich, 52425 Jülich, Germany, **2** Fakultät Angewandte Naturwissenschaften, Hochschule für angewandte Wissenschaften Coburg, 96450 Coburg, Germany, **3** Institut für Physikalische Biologie, Heinrich-Heine-Universität Düsseldorf, 40225 Düsseldorf, Germany, **4** Neurochemistry Laboratory and Biobank, VU University Medical Center Amsterdam, The Netherlands

* d.willbold@fz-juelich.de



OPEN ACCESS

Citation: Rudolph S, Klein AN, Tusche M, Schlosser C, Elfgen A, Brener O, et al. (2016) Competitive Mirror Image Phage Display Derived Peptide Modulates Amyloid Beta Aggregation and Toxicity. *PLoS ONE* 11(2): e0147470. doi:10.1371/journal.pone.0147470

Editor: Salvador Ventura, Universitat Autònoma de Barcelona, SPAIN

Received: October 5, 2015

Accepted: January 4, 2016

Published: February 3, 2016

Copyright: © 2016 Rudolph et al. This is an open access article distributed under the terms of the [Creative Commons Attribution License](https://creativecommons.org/licenses/by/4.0/), which permits unrestricted use, distribution, and reproduction in any medium, provided the original author and source are credited.

Data Availability Statement: All relevant data are within the paper.

Funding: D.W. was supported by grants from the "Portfolio Technology and Medicine", the "Portfolio Drug Re-search" and the Helmholtz-Validierungsfonds of the "Impuls und Vernetzungsfonds der Helmholtzgemeinschaft". This project was also supported by the TT-Fonds of the Technology Transfer Department of the Forschungszentrum Jülich.

Abstract

Alzheimer's disease is the most prominent type of dementia and currently no causative treatment is available. According to recent studies, oligomeric species of the amyloid beta (A β) peptide appear to be the most toxic A β assemblies. A β monomers, however, may be not toxic per se and may even have a neuroprotective role. Here we describe a competitive mirror image phage display procedure that allowed us to identify preferentially A β _{1–42} monomer binding and thereby stabilizing peptides, which destabilize and thereby eliminate toxic oligomer species. One of the peptides, called Mosd1 (monomer specific d-peptide 1), was characterized in more detail. Mosd1 abolished oligomers from a mixture of A β _{1–42} species, reduced A β _{1–42} toxicity in cell culture, and restored the physiological phenotype in neuronal cells stably transfected with the gene coding for human amyloid precursor protein.

Introduction

Dementia counts for more than 30 million patients worldwide. Alzheimer's disease (AD) is the most frequent type of dementia and therefore contributes largely to this number [1, 2]. Because age is the most important risk factor for AD, the number of AD patients is expected to increase further.

AD is a progressive type of dementia with symptoms like memory loss, apathy, depression, anxiety and behavioral changes as well as neuropathological hallmarks including inflammation, neuronal cell death and loss of brain mass [2–6]. To date, AD can only be treated palliatively and symptomatically, although with only limited success. Throughout our life time, A β is constantly produced from the amyloid precursor protein (APP) by β - and γ -secretases [7, 8].

Currently, soluble A β oligomers are assumed to be the major toxic species in AD [9–11]. A β oligomers were shown to account already at nanomolar concentrations for neuronal atrophy,

Competing Interests: The authors have declared that no competing interests exist.

induction of synaptic dysfunction, formation of pores and thereby disturbance of cellular ion homeostasis and inhibition of long-term potentiation, altogether leading to impaired neuronal function, reduced cognition and a decline in memory [12–16]. The conversion between the different A β assembly states is dynamic and reversible [13, 14, 17–22]. Recent research gave rise to the fact that AD might be a prion-like disease with misfolded A β molecules acting as nucleation seeds and initiating aggregate formation by recruiting additional unfolded or oligomeric A β peptides and thereby accelerating amyloid growth [23, 24].

From the current point of view, elimination of A β oligomers may be the most promising therapeutic intervention to AD. Our approach was to identify therapeutically interesting compounds by selection of ligands, which modulate the dynamic equilibrium of A β_{1-42} species towards decomposition of toxic oligomers by binding of the ligand to monomeric A β and stabilizing it within the equilibrium and thereby shifting the equilibrium away from A β oligomers.

Phage display selection is suitable to identify small peptide ligand that bind to any target, for example, A β . The variation of phage display using the exact mirror image of the original target is called mirror image phage display. This method allows the identification of peptides that consist solely of D-enantiomeric amino acid residues [25, 26]. Such D-peptides are more protease-resistant than peptides consisting of L-enantiomeric amino acid residues and have a prolonged half-life in the body [27–30]. Additionally, D-peptides are assumed to show lower immunogenicity even though immunogenicity levels may depend on the dose and frequency of administration [27–29, 31, 32].

Previously, we have shown that the D-peptide D3, which was derived from a mirror image phage display selection, is able to reduce the amyloid plaque load in transgenic mice, improve cognition and reduce inflammation after oral application [33, 34]. This has proven the suitability of mirror image phage display to identify highly active compounds that are stable enough for oral administration.

Here, we set out to repeat this successful strategy, but with an important modification to yield small, D-enantiomeric peptides that show increased specificity for A β monomers in order to stabilize them. Based on a previously described combination of selection and counterselection [35] we used D-enantiomeric A β_{1-42} monomers as bait and added A β_{1-42} oligomers and fibrils as counterselective agents to achieve our goal.

Materials and Methods

Peptides

Mosd1 (ysylsyhmwvr-NH₂, all amino acids are D-enantiomers) with > 98% purity was purchased from peptides & elephants (Potsdam, Germany). N-terminally biotinylated and non-biotinylated D-enantiomeric A β_{1-42} was purchased from JPT (Berlin, Germany), N-terminal biotinylated L-enantiomeric A β_{1-42} was purchased from AnaSpec (Fremont, CA, USA) and L-enantiomeric A β_{1-42} was acquired from Bachem (Bubendorf, Switzerland).

Preparation of seedless A β_{1-42} stock solutions

Generally, all A β_{1-42} preparations were handled in siliconized reaction tubes with protein low binding features (Protein LoBind tubes, Eppendorf AG, Hamburg, Germany) and prepared as seedless stock solutions as follows. A β_{1-42} was dissolved in PTFE-filtered 1,1,1,3,3,3-hexafluoro-2-propanol (HFIP) and incubated at room temperature (RT) overnight. The HFIP was evaporated in a vacuum centrifuge at RT and additionally overnight in the open reaction tube covered with a lint-free wipe. The A β_{1-42} film was dissolved in filtered HFIP to 1 mM, aliquoted, sealed with parafilm and stored at -20°C. Prior to use, HFIP was evaporated.

Separation of A β _{1–42} species via size exclusion chromatography (SEC)

In order to obtain monomeric and oligomeric A β _{1–42} fractions, size exclusion gel filtration chromatography was executed following an optimized protocol of Johansson *et al.* [36]. Seedless A β _{1–42} in HFIP was dried in a vacuum centrifuge and solved in elution buffer (50 mM sodium phosphate, 150 mM NaCl, pH 7.4) to a concentration of 250 μ M. After one minute vortexing, the sample was sonicated for one minute and centrifuged for 60 seconds at 16,000 x g to precipitate eventually undissolved remains. The supernatant was transferred in a syringe to a Superdex 75 10/300 GL column connected to an ÄKTA purifier FPLC chromatography system (both GE Healthcare Europe GmbH, Freiburg, Germany). Size exclusion was executed at a flow rate of 0.6 ml per minute and detection took place at 214 nm. The desired fractions were collected and pooled. A β _{1–42} oligomers eluted at about 8 ml and A β _{1–42} monomers at approximately 14 ml.

Preparation of A β _{1–42} samples with a broad range of different sized species

In order to gain a solution of A β _{1–42} which resembles several toxic and nontoxic A β species over a broad size range, 80 μ M seedless A β _{1–42} was incubated in 10 mM sodium phosphate buffer (pH 7.4) for 4.5 hours at RT and shaking at 600 rpm.

Preparation of A β _{1–42} fibrils

In order to gain A β _{1–42} fibrils, seedless A β _{1–42} was incubated at 80 μ M in 10 mM sodium phosphate buffer (pH 7.4) at RT for at least 24 hours with shaking at 600 rpm. To separate the fibrils from other species, the sample was loaded onto an iodixanol density gradient as described below. Fractions containing fibrils and high molecular weight (HMW) aggregates (fractions 12–14) were used for further experiments.

Density gradient centrifugation (DGC)

In order to separate differently sized A β _{1–42} assemblies, 100 μ l of the sample were added on the top of a discontinuous gradient of iodixanol (OptiPrep, AXIS-SHIELD, Oslo, Norway). The gradient was prepared by layering 260 μ l of 50% iodixanol at the bottom of a 11 x 34 mm polyallomer centrifuge tube, overlaid by 260 μ l of 40%, 260 μ l of 30%, 780 μ l of 20%, 260 μ l of 10% and 100 μ l of 5% iodixanol. The samples were spun at 260,000 x g for three hours at 4°C in an Optima MAX-XP ultracentrifuge with a TLS-55 rotor (both Beckman Instruments, Brea, USA). After centrifugation, 14 fractions of 140 μ l each were harvested with a pipette from top to bottom.

Competitive mirror image phage display

In order to obtain specifically A β _{1–42} monomer binding species, a mirror image phage display with six panning rounds was performed. To reduce binding of phages to larger A β _{1–42} species, A β _{1–42} oligomers and fibrils were added, starting from round two, as counter-selective agents. Phages binding to A β _{1–42} oligomers and fibrils were subsequently removed from the solution leading to an enrichment of phages, which exclusively bind monomeric A β _{1–42}.

The target peptide, SEC-derived monomeric, D-enantiomeric, N-terminally biotinylated A β _{1–42}, was immobilized to plates with alternating surface properties. In order to avoid selection of plastic binding phages, different plastic surfaces were used in each subsequent round of panning (Nunc 96-well Immobilizer Streptavidin microwell plate, polystyrene (Thermo Fisher Scientific Inc., Waltham, MA, USA), polypropylene and polycarbonate microwell plates

96-well (BioTeZ Berlin Buch GmbH, Berlin, Germany)). According to the manufacturer, the polystyrene plates were pretreated by washing three times with 300 μ l of 1x TBS containing 0.05% (v/v) Tween-20 per well. Additionally, in every second round, the surface was blocked with 150 μ l of 1x TBS / 0.1% (v/v) Tween-20 / 1% BSA (w/v) per well with gentle shaking for one hour at RT prior to the addition of the target peptide to reduce unspecific binding. Thus, no combination of plate surface and blocking was used twice during the six panning rounds performed.

One-hundred microliters of a 63 nM solution of target peptide diluted in 1x TBS per well was immobilized to the well for five minutes at RT, followed by three washing steps with 150 μ l of 1x TBS.

In the first panning round 90 μ l of 1x TBS were mixed with 10 μ l of the Ph.D.-12 Phage Display Peptide Library (New England Biolabs GmbH, Frankfurt/M, Germany) and added to the well for five minutes of incubation at RT. The solution was removed and 100 μ l of 10 μ M biotin in 1x TBS / 0.1% (v/v) Tween-20 (TBS-T) were added for five minutes incubation at RT to reduce streptavidin-binding phages. Subsequently, the well was washed four times with TBS-T.

Elution of bound phages was conducted by adding 100 μ l of 0.2 M glycine-HCl (pH 2.2) for ten minutes at RT. The solution was removed and subsequently added to a fresh reaction tube with 25 μ l of 1 M Tris-HCl (pH 9.1) in order to neutralize the solution. Twenty microliters of the solution were then used for phage titer determination after elution (output titer). The remaining volume was used for amplification of the eluted phages.

Determination of the output titer and phage amplification was conducted according to the distributor's manual. Shortly, 100 μ l of phage dilutions ranging from 10^{-2} to 10^{-7} were mixed with 100 μ l *E. coli* K12 ER2738 cells at an optical density of 0.6. The mixture was plated together with 800 μ l top agar per dilution on LB/Tet/IPTG/XGal Petri dishes (40 x 10 mm) and incubated overnight at 37°C. The next day, plaques were counted and the titer was determined.

For phage amplification, 20 ml *E. coli* K12 ER2738 cell solution were grown to an optical density of 0.1 and incubated with the remaining volume of eluted phages (105 μ l) for 4.5 hours at 37°C and 160 rpm. After incubation, the culture was centrifuged for 20 minutes at 2,300 x g at 4°C and 1 ml of the supernatant was removed and stored at 4°C. The remaining volume was precipitated overnight at 4°C with 7 ml PEG-8000 / 2.5 M NaCl. Subsequently, the solution was centrifuged for 60 minutes at 3,000 x g and 4°C whereupon the supernatant was discarded. After dissolving the pellet in 1 ml of 1x TBS, the sample was centrifuged for five minutes at 9,300 x g at 4°C. The supernatant was mixed with 200 μ l PEG-8000/2.5 M NaCl, followed by 60 minutes incubation on ice and a final centrifugation step for 20 minutes at 16,000 x g and 4°C. The supernatant was removed and the pellet was resuspended in 100 μ l of 1x TBS. The input titer was measured analogically to the output titration with dilutions ranging from 10^{-8} to 10^{-13} .

While the concentration of the target peptide remained stable, D-enantiomeric A β_{1-42} oligomers and high molecular weight (HMW) aggregates/fibrils without an N-terminal biotin tag were added, starting from panning round two in increasing concentrations (round 2: 1 nM—round 3: 5 nM—round 4: 10 nM—round 5: 50 nM—round 6: 500 nM) as will be explained below. A β_{1-42} oligomers and HMW aggregates and fibrils were obtained from SEC and DGC, respectively, as described above. In order to obtain A β_{1-42} HMW aggregates and fibrils fractions 12, 13 and 14 from the DGC were combined. Due to the addition of the competition step with A β_{1-42} oligomers and HMW aggregates/, the protocol was adjusted starting from the second panning round as follows. The amplified phages from the previous round were diluted to 1×10^{11} phages in 60 μ l of 1x TBS and added to the well previously coated with SEC-derived, D-enantiomeric, N-terminally biotinylated A β_{1-42} monomers. Twenty microliters of SEC-derived A β_{1-42} oligomers and 20 μ l of DGC-separated A β_{1-42} HMW / fibrils, each diluted in 1x TBS to

the above mentioned concentration (e.g. for the second panning round 1 nM and 5 nM for panning round 3), were additionally added to the sample. After five minutes of incubation at RT, the solution was removed and the procedure went on with the aforementioned biotin competition step. The amount of washing steps increased with every panning round (4–6–8–10–12–15).

Single phage amplification

Single plaque forming units, each representing phages grown from one single clone, were picked from the output titer plates from round three to six and added to 5 ml of a *E. coli* K12 ER2738 culture at an optical density of 0.1 grown in LB/tetracycline medium and were then amplified for 4.5 h hours at 37°C at 160 rpm. Cultures were centrifuged for 20 minutes at 3,000 x g and 4°C and the supernatant was removed. Two milliliters were used for DNA extraction and kept at 4°C until usage, one milliliter was aliquoted for single phage ELISA and 0.5 ml were mixed with 0.5 ml 80% sterile glycerin as backup and stored at -80°C.

Single phage ELISA

The specificity and affinity of single phage clones towards the target peptide and the counterselective agents A β _{1–42} oligomers and HMW aggregates / fibrils was analyzed by ELISA.

320 nM of SEC-derived N-terminally biotinylated D-A β _{1–42} monomers or 320 nM SEC-derived N-terminally biotinylated D-A β _{1–42} oligomers mixed with DGC-derived N-terminally biotinylated A β _{1–42} HMW aggregates/fibrils were immobilized in duplicates for each single phage clone. Therefore, the total amount of A β _{1–42} in each well was 150 ng. Amplified single phage clones from panning rounds three to six were analyzed. Additionally, the different species were immobilized to two wells each in order to check the immobilization efficiency by the A β -specific antibody 6E10 (Beta Amyloid 1–16 (6E10) monoclonal antibody, BioLegend, Dedham, MA, USA). Non-coated wells were used as additional controls for each phage. Additionally, buffer instead of phages was applied as control for cross reactivity of the anti M13:HRP conjugated antibody to the well surface and the immobilized target in duplicate.

The microtiter plates (Nunc 96-well Immobilizer Streptavidin microwell plate, Thermo Fisher Scientific Inc., Waltham, MA, USA) were pretreated as recommended by the manufacturer. The aforementioned A β _{1–42} species were diluted in 1x TBS to 320 nM each and 100 μ l per well were incubated for 15 minutes at RT with gentle shaking. After washing the wells twice with 150 μ l of 1x TBS and blocking for one hour at RT with 1% (w/v) BSA in TBS-T, the plates were washed again three times with 150 μ l of TBS-T. During the blocking step, the amplified phages and the buffer control (LB medium) were mixed with 1% (w/v) BSA in TBS-T in a ratio of 1:1 and incubated on a shaker at RT for 20 minutes. Afterwards 100 μ l of the phage suspensions, the buffer control and the first antibody solution (6E10 1:1,000 in TBS-T) were given to the wells for one hour with gentle shaking at RT. After washing the plates for five times with 150 μ l of TBS-T, 200 μ l of TBS-T were added to each well and the plates were incubated at RT for another hour.

The supernatant was removed and 100 μ l of the antibody dilutions were added to the adequate wells for one hour at RT (mouse anti bacteriophage M13 major coat protein (p8) HRP conjugated, GE Healthcare Europe GmbH, Freiburg, Germany and goat anti mouse IgG (H+L) HRP conjugated, Thermo Fisher Scientific Inc., Rockford, IL, USA, respectively). The anti-M13 antibody was diluted 1:5,000 in TBS-T and the goat anti mouse IgG antibody was diluted 1:1,000 in the same buffer. Subsequently, the plates were washed ten times with 150 μ l of TBS-T and detection was conducted by measuring the conversion of the substrate 3,3',5,5'-tetramethylbenzidine (TMB) by HRP accompanied with a color change. Therefore, 50 μ l of a

TMB solution (one pill TMB was dissolved in 1 ml DMSO and diluted with 9 ml sterile filtered 0.05 M phosphate citrate buffer) was added to each well and color change was stopped by adding 50 μ l of 2 M H₂SO₄ when the solution in the wells started getting turquoise. The absorption at 450 nm was measured in a microplate reader. After subtraction of the buffer control, the absorption at 450 nm for the wells coated with A β _{1–42} oligomers and fibrils were normalized to the A β _{1–42} content of the A β _{1–42} monomer-coated wells as determined by 6E10.

DNA extraction for sequencing

The single stranded phage DNA was purified as described in the NEB phage display manual (Instruction manual, version 2.7) with the exception that the iodide buffer was exchanged by a 10:1 mixture of 3M sodium acetate (pH 5.2) and TE buffer. Sequencing was conducted by GATC Biotech AG (Konstanz, Germany).

Transmission electron microscopy (TEM)

In order to analyze which A β _{1–42} species have formed after incubation with the peptide Mosd1, TEM images were taken. Ten micromolar seedless A β _{1–42} was incubated with or without 10 μ M Mosd1 for 24 hours at RT. Twenty microliters of each sample were spotted on a formvar/carbon coated copper grid (Plano GmbH, Wetzlar, Germany) for three minutes. Afterwards the solution was detached with filter paper and the grids were washed three times with 20 μ l of ddH₂O and once with 5 μ l 1% aqueous uranyl acetate. Then, 5 μ l of the 1% uranyl acetate solution was applied to the grid for one minute for negative staining. The solution was removed and grids were dried overnight. The samples were analyzed with a Libra 120 transmission electron microscope (Carl Zeiss AG, Oberkochen, Germany) operating at 120 kV.

Quantitative determination of interference with A β _{1–42} aggregate size distribution

The density gradient centrifugation method allows matrix-free separation and fractionation of different A β _{1–42} species according to their sedimentation coefficients which depend on size and shape.

A β _{1–42} was incubated as mentioned above (250 μ l 80 μ M seedless A β _{1–42} in 10 mM sodium phosphate buffer at pH 7.4, 4.5 hours, 600 rpm, RT) in order to gain a mixture of differently sized species. In order to analyze the influence of Mosd1, coinubation for 40 minutes at RT with different concentrations of the peptide (0–10–20–40–80 μ M) followed.

One-hundred microliters were given on the top of a discontinuous iodixanol gradient and spun in an ultracentrifuge as described above. Fourteen fractions of 140 μ l each were harvested from top to bottom after centrifugation and the residual pellet (60 μ l) was mixed with 60 μ l of 6 M guanidine hydrochloride and boiled for ten minutes. This sample represents the 15th fraction. The samples were analyzed by RP-HPLC and Tris-tricine SDS-PAGE followed by silver staining.

Peptides were quantified via isocratic reversed-phase high performance liquid chromatography (RP-HPLC). The column used was a Zorbax SB-300-C8 on a 1260 Infinity system (both Agilent Technologies Deutschland GmbH, Böblingen, Germany). Twenty microliters of each sample were injected and run with 1 ml per minute in an aqueous 30% (v/v) acetonitrile / 0.1% (v/v) trifluoroacetic acid buffer as mobile phase and 80°C column temperature to denature A β species and separate them from other components, especially iodixanol. The signal was detected at an absorbance of 214 nm. The data were recorded and peaks were integrated using the ChemStation software (Agilent Technologies). In order to calibrate the column, A β _{1–42} solutions of

known concentration were used to plot peak area versus $A\beta_{1-42}$ concentration. The plot equation then allowed calculation of $A\beta_{1-42}$ concentration within the samples.

Seeding assay (ThT)

In order to analyze the influence of Mosd1 on seeded growth of $A\beta_{1-42}$, the seeding potential of fibrillary $A\beta_{1-42}$ seeds on seedless $A\beta_{1-42}$ was monitored via Thioflavin T (ThT) fluorescence.

Seedless $A\beta_{1-42}$ (200 μM in 10 mM sodium phosphate buffer) were incubated at 37°C and 600 rpm for three days in order to gain seeding-competent $A\beta_{1-42}$ fibrils. The sample was centrifuged at 14,000 $\times g$ for 45 minutes at 4°C in order to sediment fibrillary $A\beta_{1-42}$ content. The supernatant was removed and the remaining $A\beta_{1-42}$ fibrils were diluted in 100 μl 10 mM sodium phosphate buffer. After sonication for two minutes, concentration was determined by RP-HPLC. $A\beta_{1-42}$ seeds were incubated with or without a fivefold molar excess of Mosd1 for additional 24 hours. The mixture of $A\beta_{1-42}$ seeds and Mosd1 was again sonicated for two minutes and added to freshly prepared seedless $A\beta_{1-42}$ (15 μM) and 20 μM ThT. The final concentrations were 1.88 μM $A\beta_{1-42}$ seeds and 9.4 μM Mosd1. Each sample was added to a 96-well microtiter plate in triplicate and progression of fluorescence values was monitored over time at 24°C. The experiment was conducted independently for three times.

For each sample an asymmetric five parameter fit was used in order to determine the amplitude of relative fluorescence units and the half-life $t_{1/2}$. After checking for Gaussian distribution by D'Agostino-Pearson omnibus normal test, significance was determined by one-way ANOVA.

Cell viability assay (MTT reduction)

PC-12 cells (DSMZ-Deutsche Sammlung von Mikroorganismen und Zellkulturen GmbH, Braunschweig, Germany) were cultured in DMEM medium supplemented with 10% fetal calf serum, 1% antibiotics (Penicillin / Streptomycin) (all Sigma-Aldrich Corp., St. Louis, MO, USA) and 5% horse serum (PAA Laboratories GmbH, Pasching, Germany) on collagen A-coated (Biochrom GmbH, Berlin, Germany) tissue culture flasks (SPL Life Sciences Co., Korea) in a humidified incubator with 5% CO_2 at 37°C and grown for a maximum of 15 passages. Medium was changed every two days and cells were passaged, according to their confluence, every three to five days.

PC-12 cells were seeded in clear, collagen-coated 96-well flat bottom microwell plates (Life Technologies Inc., Carlsbad, CA, USA) at a density of 1×10^4 cells in a volume of 100 μl per well and incubated for 24 hours. $A\beta_{1-42}$ / Mosd1 mixtures were incubated as already described in the above mentioned assay for quantitative determination of interference with $A\beta_{1-42}$ aggregate size distribution. Mosd1 concentrations of 0/40/80 μM were used. From each well that contained cells 1.25 μl medium were removed and replaced with 1.25 μl of the preparations in order to gain a final concentration of 1 μM $A\beta_{1-42}$ and 0/1/0.5 μM Mosd1 in every well, respectively. Every approach was tested three times at least in quintuplicates. The plates were incubated for 24 hours in the incubator with 5% CO_2 at 37°C. Subsequently, 10 μl of the supernatant were taken out of every well and 10 μl of MTT reagent (Cell proliferation kit 1, Roche Diagnostics GmbH, Mannheim, Germany) were added for four hours of incubation in the incubator. Afterwards, 100 μl of solubilization reagent (Roche Diagnostics GmbH, Mannheim, Germany) were added to all wells and the plate was incubated overnight. The plate was shaken on a table shaker for five minutes to distribute the purple colored solution equally within each well and absorbance was measured at 660 nm and 570 nm with a microplate reader (POLARstar OPTIMA, BMG Labtech GmbH, Ortenberg, Germany). Reference values at 660 nm were subtracted from values for formazan absorbance (570 nm). The mean value of cell-free wells was subtracted as background. The arithmetic mean of all measurements per approach was calculated. Results are

represented as the percentage of MTT reduction, assuming that the absorbance of control cells was 100%. Cells treated with 0.1% TritonX-100 in 10 mM sodium phosphate buffer (pH 7.4) served as control for dead cells. After analysis for Gaussian distribution by Shapiro-Wilk test, the values were tested for significance using the Mann-Whitney *U* test.

Western blot to investigate γ -secretase inhibition

Neuro-2a cells (DSMZ, Braunschweig, Germany) and Neuro-2a cells stably transfected with human APP695 were cultured in DMEM with 10% fetal calf serum and 1x non-essential amino acids (both Sigma-Aldrich Corp., St.Louis, MO, USA) in tissue culture flasks in a humidified incubator with 5% CO₂ at 37°C. Fifty thousand cells per well were seeded in 500 μ l in a 24 well microwell plate for 24 hours at 37°C and 5% CO₂ to assure attachment to the surface. A stock solution of 1 mM Mosd1 was prepared in sterile water and the γ -secretase inhibitor DAPT was diluted to 5 mM in DMSO, respectively. The dilutions were spun at 1,000 x g for one minute prior to use. Then 0/10/100 μ M Mosd1 and 1 μ M DAPT were added to the cell supernatant and DMSO as well as water were tested as control. The cells were incubated at 37°C and 5% CO₂ for 24 hours. The cells were analyzed with a laser scanning microscope LSM 710 (Carl Zeiss AG, Oberkochen, Germany). Afterwards, the cells were washed three times with 1x PBS and lysed with 60 μ l of NP-40 lysis buffer for 15 minutes. The lysates were resuspended, transferred to reaction tubes and centrifuged for five minutes at 12,000 x g. Afterwards, the supernatants were transferred to new reaction tubes and protein concentration was determined via microBCA assay.

For gel electrophoresis the lysates were adjusted to the lowest measured protein concentration. All samples were mixed with 4x Tris-tricine gel loading buffer (4% SDS (w/v), 12% Glycerin (v/v), 50 mM Tris, 2% β -mercaptoethanol (v/v), 0.01% SERVA BlueG (w/v); pH 6.8) in a ratio of 1:3 and boiled for ten minutes. Gel electrophoresis was conducted with 10% Tris-tricine gels at a constant voltage of 120 V. The PageRuler prestained protein ladder 10–170 kDa (Thermo Fisher Scientific, Inc., Rockford, IL, USA) served as marker.

After gel electrophoresis, the proteins were transferred via semi-dry blotting to a PVDF membrane. Protein transfer took place at 1 A and 25 V for 30 minutes. The membrane was blocked with 5% non-fat dry milk powder in 1x TBS-T at 4°C overnight with gentle shaking. Subsequently, the membrane was washed three times with TBS-T at RT and gentle shaking. The primary antibody for the detection of C-terminal fragment of APP (anti-amyloid precursor protein, C-terminal (751–770) rabbit pAb, Merck KGaA, Darmstadt, Germany) was diluted 1:5,000 in TBS-T. Simultaneously, the anti- β -actin antibody (β -actin (8H10D10) mouse mAb, Cell Signaling Technology, Inc., Danvers, MA, USA) was diluted 1:1,000 in TBS-T and both antibodies were given to the membrane, which was incubated overnight at 4°C on a roller mixer, subsequently. The membrane was washed three times with TBS-T and incubated with the secondary antibodies goat anti-rabbit IgG:HRP diluted 1:5,000 in TBS-T and goat anti-mouse IgG:HRP diluted 1:10,000 in TBS-T (both Santa Cruz Biotechnology, Inc., Dallas, Texas, USA) for three hours at RT on a roller mixer. After three washing steps with TBS-T, the membrane was incubated with the substrate for enhanced chemoluminescence (SuperSignal West Dura Chemoluminescent Substrate, Thermo Fisher Scientific, Inc., Rockford, IL, USA) for five minutes at RT in the dark. The signal was detected with the ChemiDoc MP gel documentation system (Bio-Rad Laboratories, Inc., Hercules, CA, USA).

Results

N-terminally biotinylated, SEC-derived A β _{1–42} monomers were immobilized to streptavidin-coated microwell plates. To avoid selection of plastic binding ligands, different plastic surfaces

were used in each round. In particular, polystyrene, polypropylene and polycarbonate served as surface, alternating every round. Additionally, in every second round, the surface was blocked with BSA. Due to this procedure, six different combinations of blocking and surface type were used during the panning rounds and not a single combination occurred twice. This step was important, because only very low concentrations of $A\beta_{1-42}$ were immobilized in order to assure its monomeric state. Thus, there was a substantial risk that uncoated surface may have a strong bias during selection. In the first panning round, only $A\beta_{1-42}$ monomers were offered to the naïve library of phages. For the next round, amplified phages from the previous round were added together with increasing concentrations of non-biotinylated counterselective $A\beta_{1-42}$ species (SEC-derived oligomers and DGC-derived HMW aggregates and fibrils). After panning, a biotin competition step was conducted to remove phages that compete with biotin. Afterwards the well was washed every round with increasing rigor and still bound phages were eluted and amplified.

We verified the state of all used $A\beta$ conformers by DGC followed by Tris-tricine-SDS-PAGE and silver staining. SEC-derived $A\beta_{1-42}$ monomers, SEC-derived oligomers, and fibrillary $A\beta_{1-42}$ were analyzed. As shown in Fig 1, prepared monomers are indeed free of any aggregates, as only the most upper fractions 1 and 2 of the DGC gradient contained $A\beta$. Oligomers can be found predominantly in fractions 4 to 6, and in smaller amounts also in neighboring fractions. Fibrils can be found in the extreme high molecular weight fractions, but obviously, during the DGC run, a substantial fraction of monomers dissociated from them and can be found in fractions 1 and 2.

Single phage clones from round three to six were amplified and sequenced. Sixteen sequences occurred more than once and were therefore tested for binding to monomeric $A\beta_{1-42}$, $A\beta_{1-42}$ oligomers and HMW aggregates / fibrils as well as non-coated wells in a single phage ELISA. Additionally, several clones with uniquely occurring sequences and four clones from a previously conducted mirror image phage display were tested. This former mirror image phage display was conducted with almost identical conditions. The experimental setup differed only in two details. Firstly, the counterselective $A\beta_{1-42}$ HMW aggregates and fibrils were derived from an iodixanol gradient with different iodixanol concentrations (30–24–18–12–6 and 3% iodixanol instead of 50–40–30–20–10 and 5%). Secondly, the neutralization of the eluate took place in the same well as the elution step.

Fig 2 shows the immobilization efficiency of different $A\beta_{1-42}$ species detected by $A\beta_{1-42}$ specific antibody 6E10. On all plates used for single phage ELISA, $A\beta_{1-42}$ monomers and oligomers/fibrils were immobilized in an amount which allowed normalization of the $A\beta_{1-42}$ oligomer/fibril content to the content of $A\beta_{1-42}$ in $A\beta_{1-42}$ monomer-coated wells as determined by 6E10. As shown in Fig 3, the competitive mirror image phage display selection indeed yielded phages that display peptides that specifically bind to $A\beta_{1-42}$ monomers as demonstrated by the strong binding to $A\beta_{1-42}$ monomer coated wells and notably less binding to wells coated with $A\beta_{1-42}$ oligomers and HMW aggregates or fibrils. We picked the clone with the highest signal intensity for monomeric $A\beta_{1-42}$, but also the highest specificity for monomeric $A\beta_{1-42}$ as deduced from the high ratio of binding to $A\beta_{1-42}$ monomers and binding to oligomeric and fibrillary $A\beta_{1-42}$. The amino acid sequence of the chosen clone 5.60 was YSYLT-SYHMVWR. The corresponding D-enantiomeric peptide, named Mosd1 (monomer specific d-peptide 1), was synthesized from purely D-amino acids with its C-terminus amidated, and was further characterized.

In order to obtain information on how Mosd1 changes $A\beta_{1-42}$ aggregation, TEM pictures were taken after 24 hours incubation of $A\beta_{1-42}$ with and without an equimolar ratio of Mosd1. The $A\beta_{1-42}$ sample without Mosd1 contained a mesh of fibrils (Fig 4A). Additionally, $A\beta$ oligomers and large aggregates (dot-like structures) were present, displaying a broad range of aggregated $A\beta_{1-42}$ species. In the sample with $A\beta_{1-42}$ and Mosd1 neither fibrils nor oligomers were

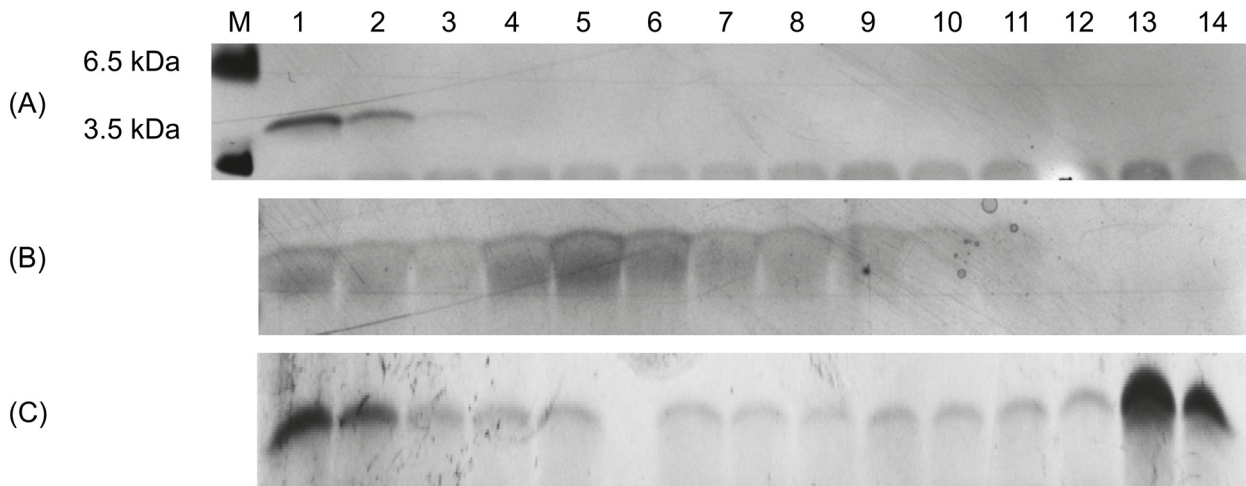


Fig 1. Silver stained Tris-Tricine-SDS-PAGE of different Aβ₁₋₄₂ species. The Aβ₁₋₄₂ species used for panning and counter selection during mirror image phage display were analyzed via DGC followed by Tris-Tricine-SDS-PAGE and silver staining. The SEC peak corresponding with Aβ₁₋₄₂ monomers (A) presents Aβ₁₋₄₂ content only in fractions 1 to 2 of a DGC gradient and therefore represents exclusively monomeric Aβ₁₋₄₂. The SEC peak corresponding with Aβ₁₋₄₂ oligomers (B) presents mainly Aβ₁₋₄₂ in fractions 4 to 6, which is in accordance with oligomeric Aβ₁₋₄₂ species. The preparation of fibrillary Aβ₁₋₄₂ resulted in monomeric and fibrillary Aβ₁₋₄₂ content as seen in fractions 1 to 2 and 13 to 14 (C). Using only the pooled fractions 12 to 14 ensured that no monomeric Aβ₁₋₄₂ species were used as counterselective agent.

doi:10.1371/journal.pone.0147470.g001

observed. Instead, amorphous, unstructured aggregates were the major species found on the grid (Fig 4B).

After incubation of 80 μM Aβ₁₋₄₂ followed by coinubation with different concentrations of Mosd1 (0/10/20/40/80 μM), samples were loaded on a discontinuous iodixanol gradient and

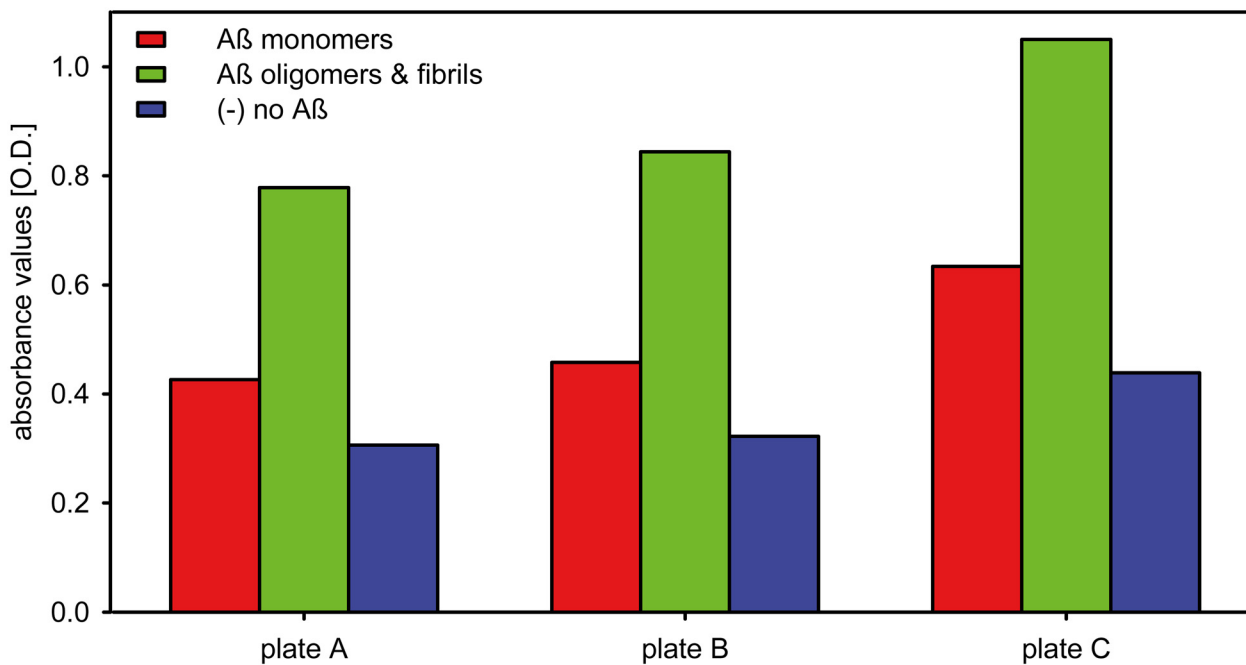


Fig 2. Single phage ELISA—immobilization control. The immobilization efficiency of different Aβ₁₋₄₂ species was analyzed by the binding affinity of Aβ₁₋₄₂ specific antibody 6E10 to immobilized Aβ₁₋₄₂ on each plate used for single phage ELISA. The Aβ₁₋₄₂ specific antibody 6E10 was added to wells coated with 150 ng Aβ₁₋₄₂ monomers (red) or 150 ng Aβ₁₋₄₂ oligomers and fibrils (1:1; green) or to wells only coated with streptavidin (blue). Transformation of substrate by the secondary antibody-conjugated HRP was measured at 450 nm.

doi:10.1371/journal.pone.0147470.g002

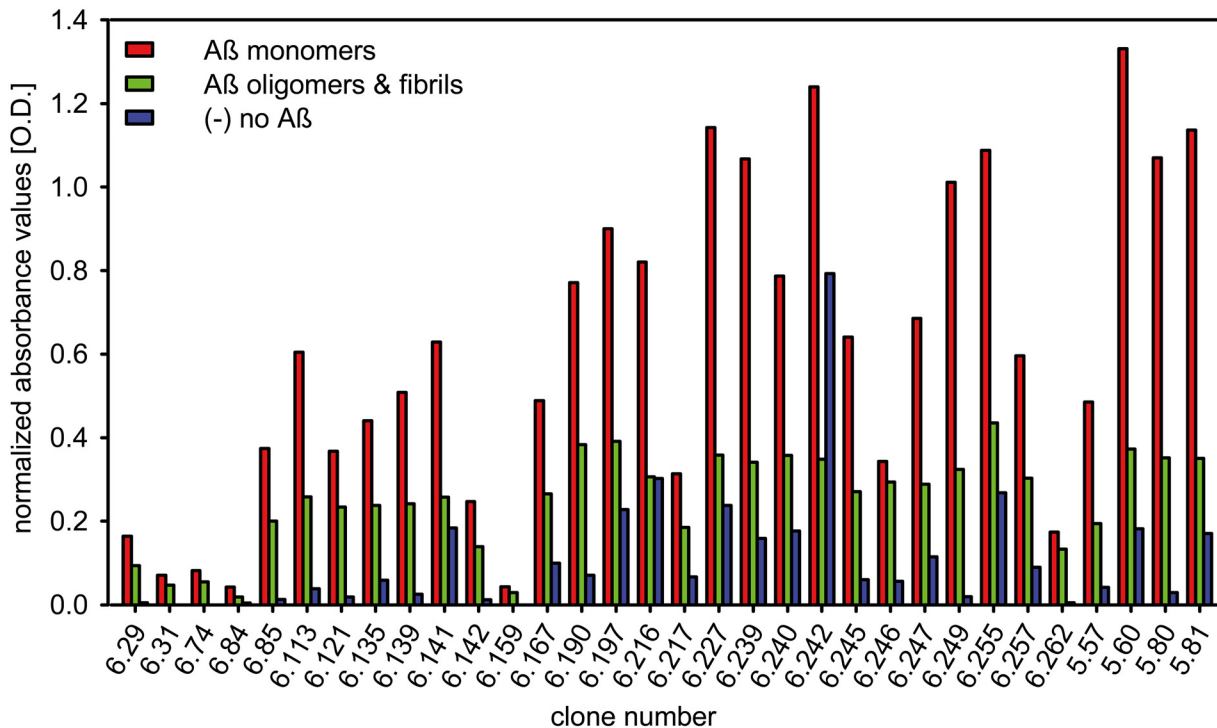


Fig 3. Single phage ELISA. The relative binding affinity of single phage clones from mirror image phage display (clone numbers 6.xx) and a previously conducted mirror image phage display (clone numbers 5.xx) to SEC-derived biotinylated Aβ₁₋₄₂ monomers, oligomers and fibrils as well as the non-coated wells was analyzed. The M13 phage-specific antibody was used for detection. Transformation of substrate by the antibody-conjugated HRP was measured at 450 nm. Amplified single phage clones were added to wells coated with 150 ng Aβ₁₋₄₂ monomers (red) or 150 ng Aβ₁₋₄₂ oligomers and fibrils (1:1; green) or to wells only coated with streptavidin (blue). Cross reactivity of the M13 phage-specific antibody was tested in an approach without addition of phages. After background subtraction of the anti M13 antibody values, the values for phage to Aβ₁₋₄₂ oligomer/fibril binding were normalized to the values of phage to Aβ₁₋₄₂ monomer binding according to the outcome of coating efficiency controls with the Aβ specific antibody 6E10.

doi:10.1371/journal.pone.0147470.g003

centrifuged. Fifteen fractions were harvested from top to bottom, applied to Tris-tricine-SDS-PAGE and silver stained. With this experiment we were able to show that Mosd1 abolishes different Aβ₁₋₄₂ species from the sample, which contains Aβ₁₋₄₂ species of different size, ranging from monomers to fibrils and HMW aggregates.

The distribution of 80 μM Aβ₁₋₄₂, incubated for 4.5 hours without addition of Mosd1, showed a broad range of species distributed from fraction 1 to 12, representing monomers, small and large oligomers, protofibrils, fibrils and HMW aggregates (Fig 5A) [37]. The amount of Aβ₁₋₄₂ as estimated from silver staining decreased with the fraction number, indicating substantial amounts of Aβ₁₋₄₂ in form of monomers and small oligomers. The most toxic oligomers can be expected in fractions four to six [38]. The addition of Mosd1 shifted the distribution of Aβ₁₋₄₂ towards large aggregates (Fig 5B-5E). This aggregates are suspected to be non-toxic [39]. The Aβ₁₋₄₂ contents in fractions one to ten were decreased with increasing Mosd1 concentrations. We therefore conclude that Mosd1 decreased the amount of toxic Aβ₁₋₄₂ oligomers and shifted the distribution equilibrium towards non-toxic aggregates in a concentration dependent manner.

Silver staining does not allow a quantitative determination of the detected species. In order to gain quantitative information about Aβ₁₋₄₂ concentrations in every fraction, samples of each fraction were applied to RP-HPLC chromatography and analyzed for their Aβ₁₋₄₂ contents, as described before [40]. The QIAD (quantitative determination of interference with Aβ₁₋₄₂ aggregate size distribution) assay fully confirmed the above described behavior of Mosd1 and

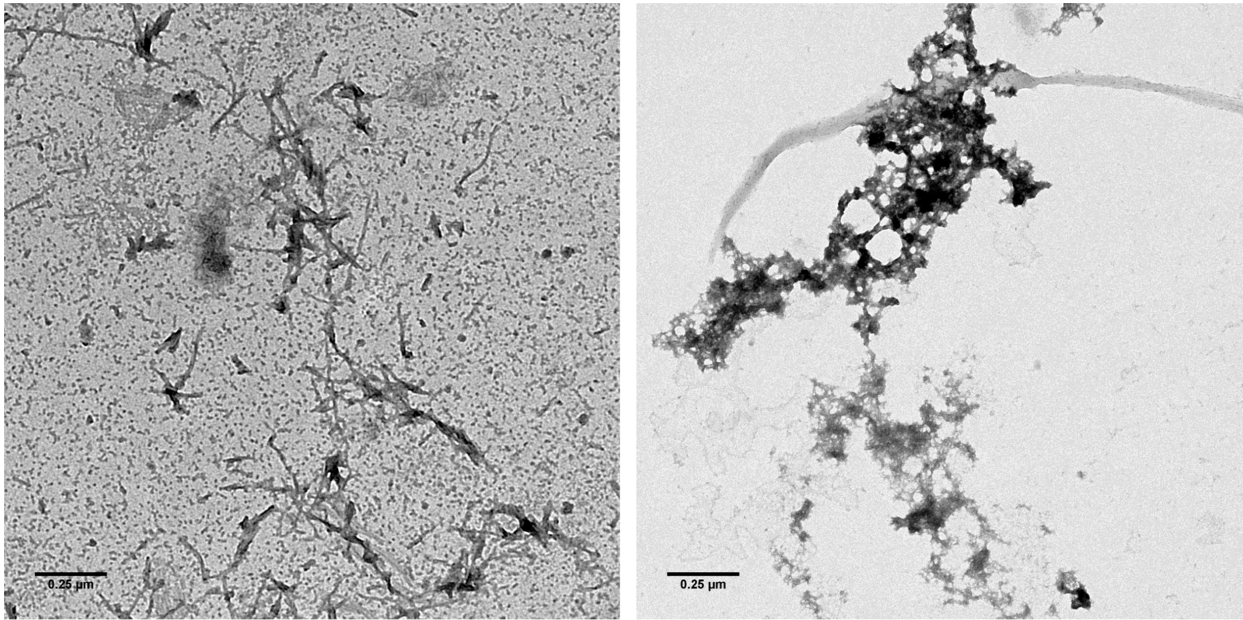


Fig 4. Transmission electron microscopy. After incubation of 10 μM pretreated $\text{A}\beta_{1-42}$ without (left picture) and with 10 μM Mosd1 (right picture) for 24 hours at room temperature, samples were spotted onto a formvar/carbon coated copper grid and stained with 1% aqueous uranyl acetate. Samples were analyzed with a Libra 120 TEM operating at 120 kV. Scale bar presents 0.25 μm .

doi:10.1371/journal.pone.0147470.g004

demonstrates that $\text{A}\beta_{1-42}$ oligomer elimination by Mosd1 is concentration dependent (Fig 6). Most importantly, Mosd1 is able to almost completely eliminate $\text{A}\beta_{1-42}$ oligomers.

A characteristic property of fibrillar $\text{A}\beta$ is to its ability to act as a seed for conversion of monomeric $\text{A}\beta$ into fibrillar $\text{A}\beta$ assemblies. We therefore analyzed the impact of Mosd1 on

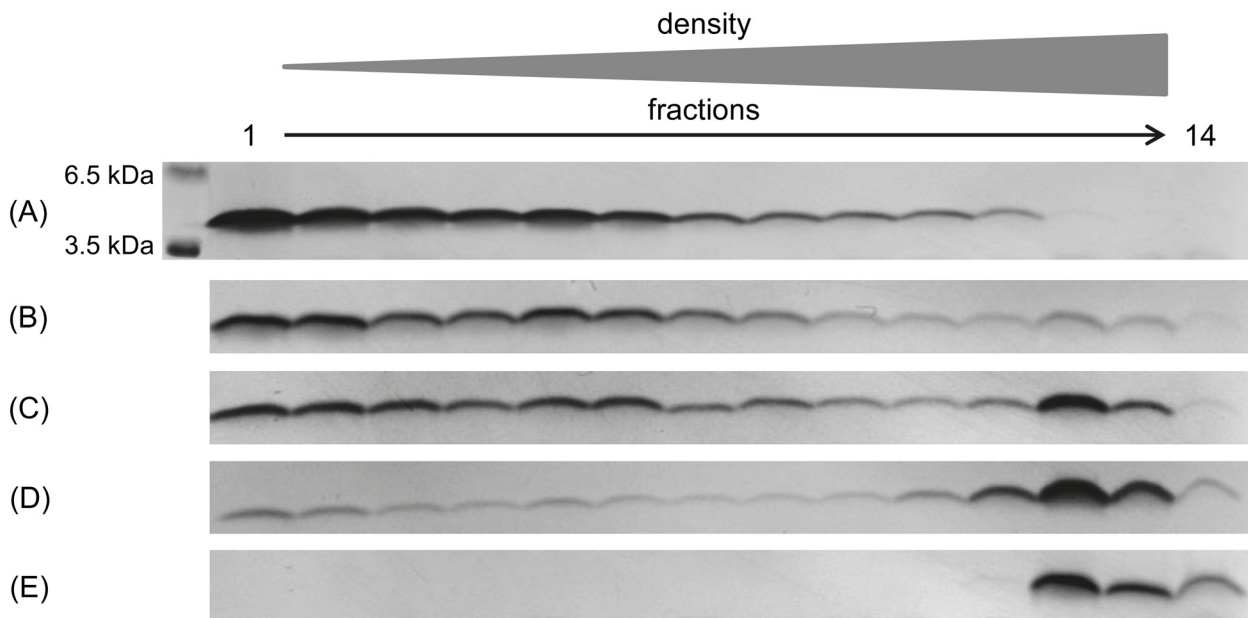


Fig 5. Qualitative $\text{A}\beta_{1-42}$ distribution alteration. Silver staining of SDS gels after incubation of 80 μM $\text{A}\beta_{1-42}$ for 4.5 hours at RT and 600 rpm and additional coincubation for 40 minutes with 0 (A) / 10 (B) / 20 (C) / 40 (D) / 80 μM (E) Mosd1 followed by density gradient centrifugation for three hours at 4°C at 259,000 x g. The bands display the signal for $\text{A}\beta_{1-42}$ (4.5 kDa).

doi:10.1371/journal.pone.0147470.g005

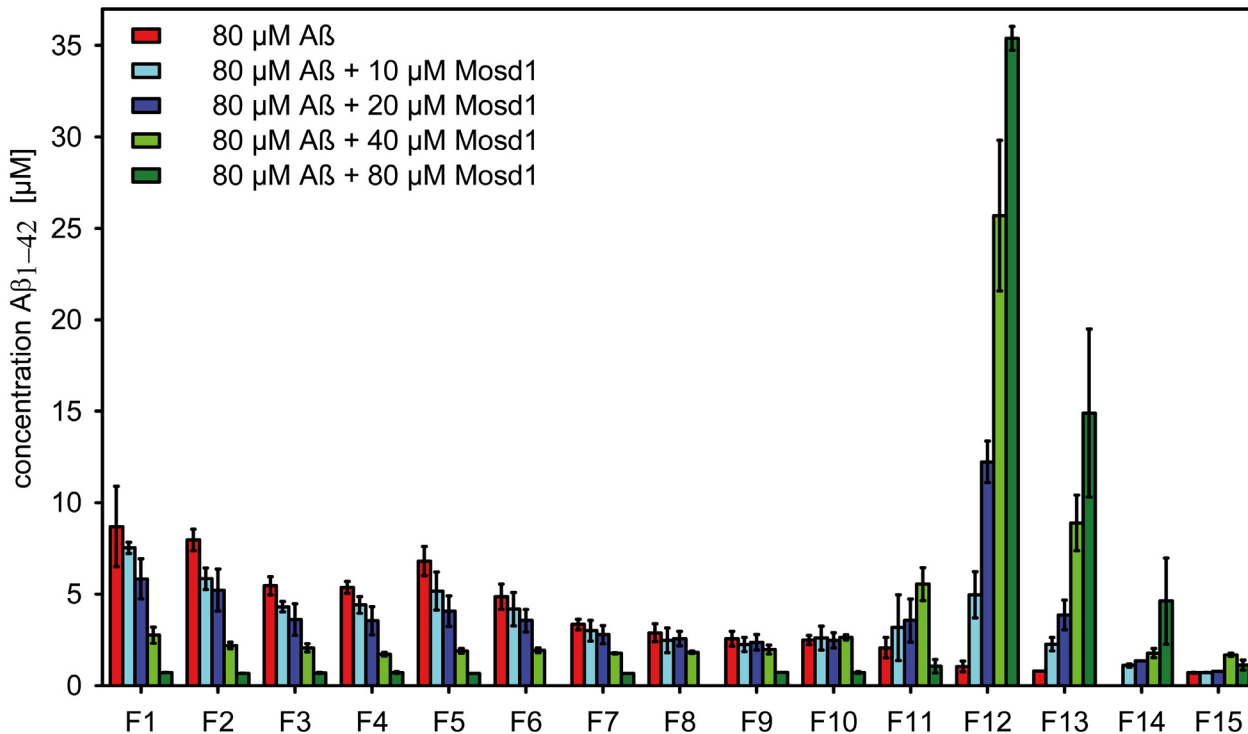


Fig 6. Quantitative concentration determination (RP-HPLC) of Aβ₁₋₄₂ distribution. Concentrations of Aβ₁₋₄₂ in each DGC fraction were determined quantitatively via RP-HPLC. Samples were loaded to a Zorbax 300SB-C8 column connected to a 1260 Infinity HPLC system. Separation of the samples was achieved by elevated column temperature (80°C) and an isocratic mobile phase of 30% acetonitrile/0.1% TFA in water. The averaged concentration of Aβ₁₋₄₂ from three independent experiments (with standard deviation) is plotted against the obtained fractions F1 to F15 of different incubation approaches of Aβ₁₋₄₂ without or with Mosd1. Shown in red are the concentrations of fractions from 80 μM Aβ₁₋₄₂ incubated without Mosd1. The following columns represent the Aβ₁₋₄₂ concentrations in the fractions from 80 μM Aβ₁₋₄₂ samples coincubated with increasing concentrations of Mosd1 (10 μM = light blue; 20 μM = dark blue; 40 μM = light green; 80 μM = dark green).

doi:10.1371/journal.pone.0147470.g006

fibril seeded fibrillation of Aβ₁₋₄₂ using the Thioflavin T (ThT) assay (Fig 7). Fibrillar Aβ₁₋₄₂ seeds were grown and afterwards incubated with or without Mosd1. ThT was added and the mixture was added to freshly prepared seedless Aβ₁₋₄₂. The progression of ThT fluorescence was monitored over time. Compared to freshly prepared seedless Aβ₁₋₄₂ (t_{1/2} = 19.69 h), addition of fibrillary Aβ₁₋₄₂ seeds significantly reduced the time needed to increase fibrillar content (t_{1/2} = 0.57 h). When fibrillary Aβ₁₋₄₂ seeds were coincubated with Mosd1 prior to addition of freshly prepared seedless Aβ₁₋₄₂, the time for the increase of fibrillary content was significantly reduced as well, yet the time for the increase was significantly longer (t_{1/2} = 3.36 h) compared to the sample without Mosd1 (Fig 7A). Furthermore, the amount of fibrillar Aβ₁₋₄₂ content in the samples, displayed by the amplitude of relative fluorescence units (Fig 7B), did differ significantly between seedless Aβ₁₋₄₂ (set to 100% RFU) and seedless Aβ₁₋₄₂ incubated with fibrillary Aβ₁₋₄₂ seeds (84%) as well as between seedless Aβ₁₋₄₂ and fibrillary Aβ₁₋₄₂ seeds coincubated with Mosd1 (74%).

In order to confirm that Mosd1 yields Aβ₁₋₄₂ species that are not toxic to cells and Mosd1 can indeed abolish the cytotoxic effect of Aβ₁₋₄₂ and rescue cell viability, an MTT assay was performed (Fig 8). PC-12 cells were incubated with Aβ₁₋₄₂ with or without different concentrations of Mosd1, derived from the same incubation method as mentioned above. Mosd1 without Aβ₁₋₄₂ was tested to ensure that Mosd1 itself is not toxic to the cells. TritonX-100 was used as

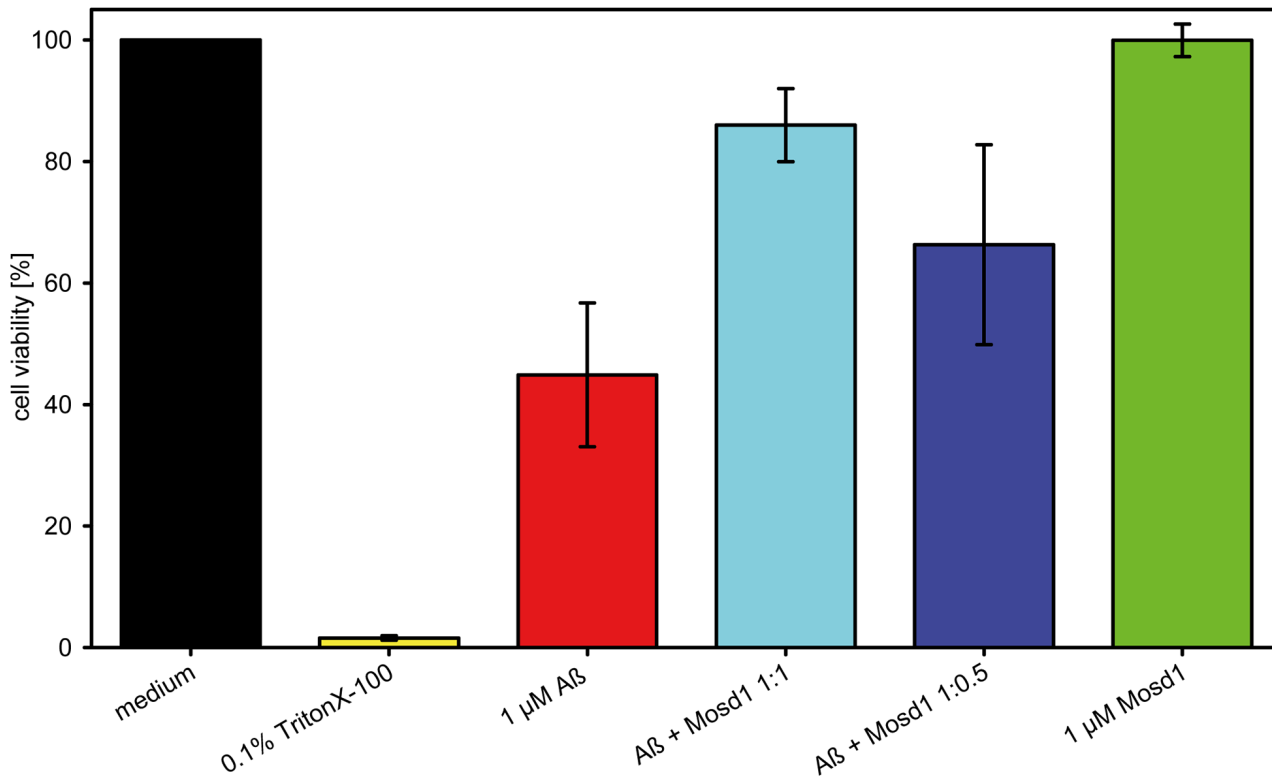


Fig 7. Reduction of seeded Aβ₁₋₄₂ growth and fibrillar Aβ₁₋₄₂ content. Seedless Aβ₁₋₄₂ was incubated alone (black) or together with fibrillary Aβ₁₋₄₂ seeds previously incubated with (green) or without (red) a fivefold molar excess of Mosd1. ThT (20 μM) was added to each sample in order to measure fibrillar content. The data were fitted with an asymmetric five parameter fit. The (A) amplitude of relative fluorescence (RFU) of fibrillated seedless Aβ₁₋₄₂ served as 100% to which the other values were normalized. The (B) half-life (t_{1/2}), displaying the point in time, when half of the maximum ThT signal (i.e. fibrillary content) was reached. Statistical significance was determined by one-way ANOVA. Error bars display SEM. ns: p > 0.05; *: p ≤ 0.05; **: p ≤ 0.01; ***: p ≤ 0.001.

doi:10.1371/journal.pone.0147470.g007

a control for cell death. Untreated cells were set 100% viable and all other values were normalized to this value. Incubation with 0.1% TritonX-100 resulted in 1.6% viable cells. The Aβ₁₋₄₂ composition led to a significantly decreased cell viability of 45% and was therefore proven to be toxic. Mosd1 in a concentration of 1 μM did not alter MTT reduction in this assay and showed no toxic effect in PC-12 cells. When coincubated with Mosd1, the toxic effect of Aβ₁₋₄₂ was significantly decreased with increasing concentrations of Mosd1. In an equimolar ratio, 86% of the cells stayed viable and with half the concentration of Mosd1 still 66% of the cells were viable. Mosd1 is therefore able to rescue PC-12 cells from Aβ₁₋₄₂ induced toxicity.

Neuro-2a cells, stably transfected with human APP695, develop a pathologic phenotype when compared with wild type Neuro-2a cells. Wild type Neuro-2a cells accumulate and grow protrusions between each other and appear polygonal, whereas Neuro-2a cells, which are stably transfected with human APP, appear isolated, spindle shaped and show less protrusions and cell contacts (Figs 9 and 10). Applied to wild type Neuro-2a cells, Mosd1 did not alter their physiological phenotype. The cells clotted and developed protrusions and appeared polygonal (Fig 9). Added to hAPP695-transfected Neuro-2a cells, Mosd1 compensated the pathological phenotype (Fig 10). The cells developed connections and protrusions, grew denser and did partially clot, resembling the phenotype of wild type Neuro-2a cells. This effect is dose dependent,

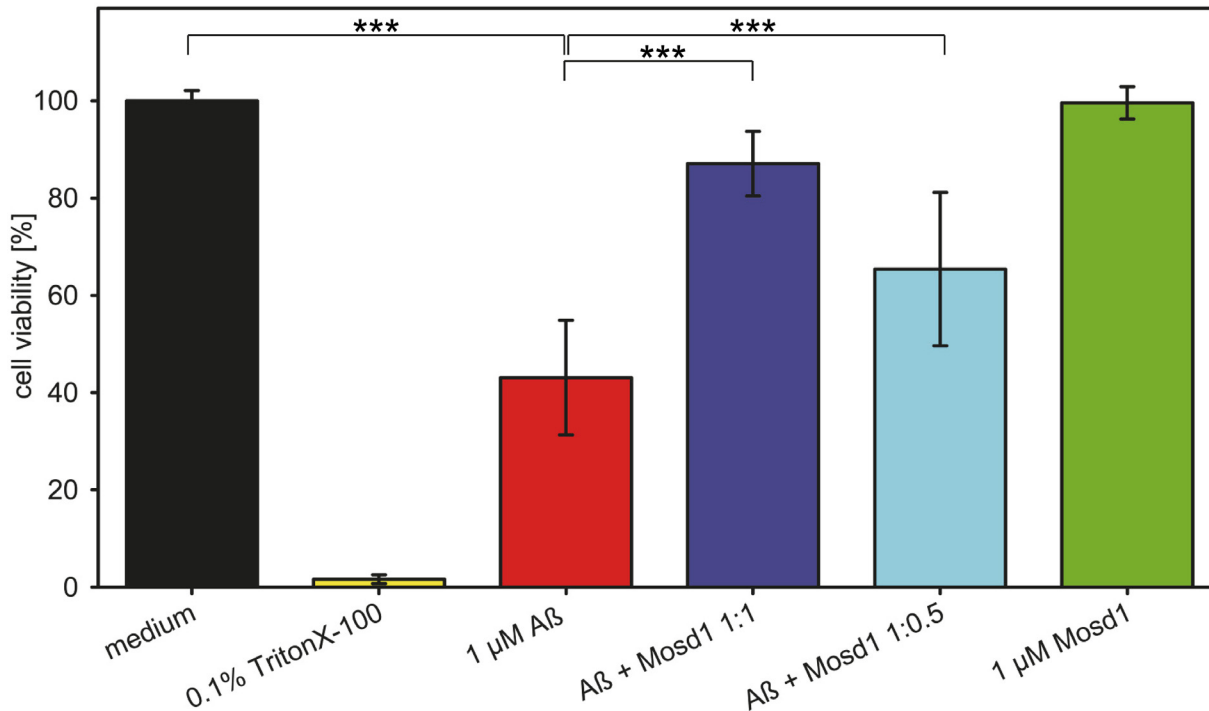


Fig 8. Effect of Aβ₁₋₄₂ and Mosd1 on cell viability. Aβ₁₋₄₂ and Mosd1 were tested for their influence on PC-12 cell viability by MTT reduction assay. Cell viability (in percent) is plotted against different treatment conditions. Adherently grown PC-12 cells were incubated 24 hours with medium (black) or 0.1% TritonX-100 (yellow) as controls for viable cells and cytotoxicity, respectively. Additionally, cells incubated for 24 hours with 1 μM Aβ₁₋₄₂ (red), Aβ₁₋₄₂ + Mosd1 1:1 (light blue) and 1:0.5 (dark blue), respectively. The green bar corresponds to cells incubated with 1 μM Mosd1 for 24 hours. Viability was analyzed by subsequent incubation with MTT substrate for four hours. After solubilization, absorbance was measured at 570 nm. The averages and standard deviations of absorbance values from five independently performed experiments were calculated and normalized to untreated cells (medium). Statistical significance was tested with Mann-Whitney *U* test. ***: $p \leq 0.001$.

doi:10.1371/journal.pone.0147470.g008

since higher concentrations of Mosd1 (10 and 100 μM) increased the development of cellular connections.

Because Mosd1 binds Aβ₁₋₄₂ monomers, it might also bind to the respective part of APP and influence its cleavage by γ-secretase. In order to investigate this potential side activity, we analyzed whether Mosd1 influences γ-secretase activity with APP as a substrate. Neuro-2a cells, stably transfected with the gene coding for human APP695 were incubated with 10 and 100 μM Mosd1, respectively. The cells were lysed, lysates were separated by SDS-PAGE, blotted and the APP C-terminal fragment β (APP CTFβ) was detected by enhanced chemoluminescence. Both concentrations of Mosd1 showed no signs of γ-secretase activity inhibition, i.e. the γ-secretase substrate APP CTFβ was not accumulated as it is the case for the treatment with the γ-secretase inhibitor DAPT (Fig 11) [41, 42].

Discussion

The competitive mirror image phage display yielded Aβ₁₋₄₂ monomer specific ligands

Our competitive mirror image phage display led to single phage clones that preferentially bind to monomeric Aβ₁₋₄₂. Sequencing of single phage clones revealed several consensus sequences which occurred multiply. Additionally, ELISA results showed an overall specificity

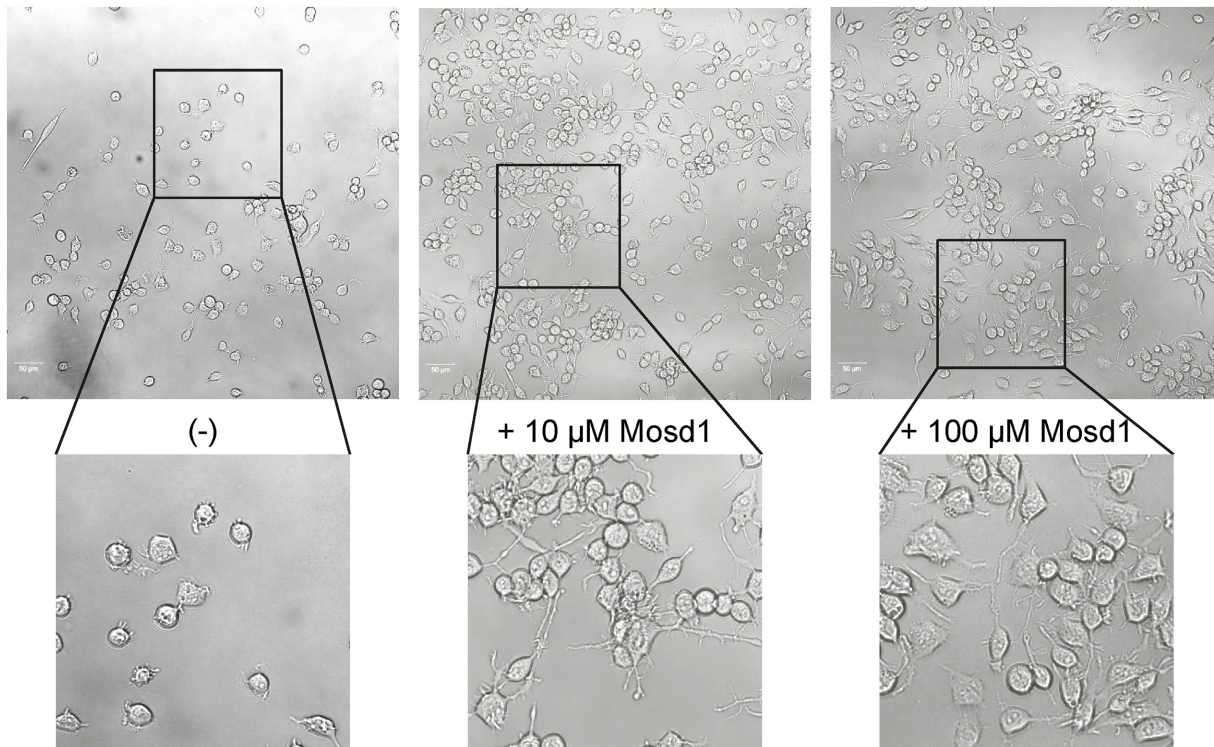


Fig 9. Effect of Mosd1 on Neuro-2a cells. Overview and detailed pictures of wild type Neuro-2a cells are shown. Neuro-2a cells were treated with 0, 10 and 100 μM of Mosd1, respectively. The left panel shows untreated wild type Neuro-2a cells. In the middle and right panel, incubation of wild type Neuro-2a cells with 10 μM Mosd1 and 100 μM Mosd1 are shown. Cell viability and morphology were analyzed with a LSM 710 laser scanning microscope. Scale bars equate 50 μm .

doi:10.1371/journal.pone.0147470.g009

of most single phage clones for monomeric $\text{A}\beta_{1-42}$ compared to $\text{A}\beta_{1-42}$ oligomers and fibrils and non-coated wells. Several single phage clones exhibited a very strong difference in binding affinities between monomeric and aggregated $\text{A}\beta_{1-42}$ and also the non-coated surface. We picked the most promising clone and investigated the respective D-peptide Mosd1 for further analysis.

Mosd1 modulates $\text{A}\beta_{1-42}$ aggregation

Via TEM and quantitative determination of $\text{A}\beta_{1-42}$ aggregate distribution, we were able to show that coinubation of $\text{A}\beta_{1-42}$ with Mosd1 leads to an altered aggregation pathway of $\text{A}\beta_{1-42}$. While incubation of $\text{A}\beta_{1-42}$ alone for 24 hours led to oligomers and fibrillar structures, coinubation with Mosd1 led to large amorphous aggregates that were shown to be non-toxic [30, 39, 40]. By combining these results with the experiment regarding interference of Mosd1 with $\text{A}\beta_{1-42}$ aggregate size distribution mentioned above, we suggest the following mode of action. Mosd1 stabilizes $\text{A}\beta_{1-42}$ monomers and thereby modulates the dynamic equilibrium of $\text{A}\beta_{1-42}$ species. Toxic $\text{A}\beta_{1-42}$ oligomers are decomposed and the resulting $\text{A}\beta_{1-42}$ species being precipitated and converted into amorphous non-toxic aggregates instead of fibrils. According to Ladwala *et al.*, Mosd1 can be sorted into class I molecules, which convert soluble $\text{A}\beta$ oligomers into large, non-toxic conformers [43]. In addition, Mosd1 with 33% residues being aromatic shares the overall aromatic features of compounds, which belong to this class. Indeed, also polyphenols like resveratrol and derivatives or polyphenolic flavones like kaempferol-3-O-rhamnoside are able to cause the development of large, non-toxic, off-pathway $\text{A}\beta$ aggregates

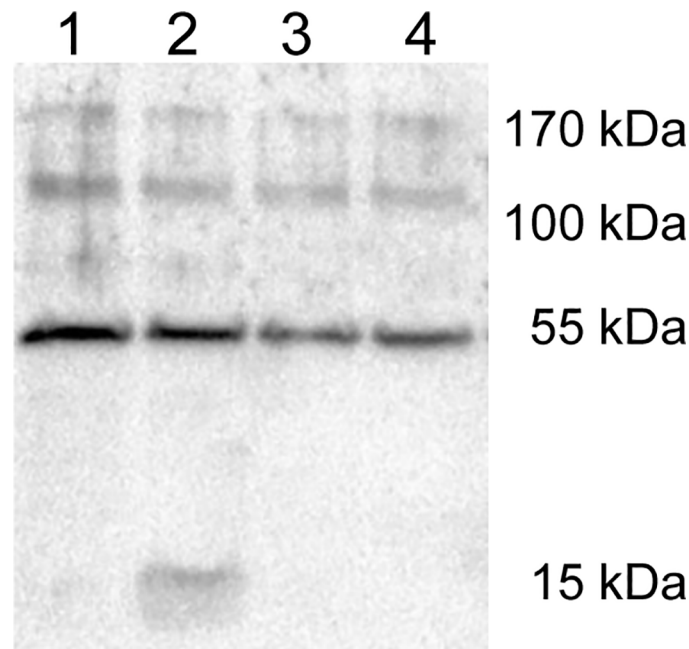


Fig 10. Effect of Mosd1 on Neuro-2a cells stably transfected with human APP695. Overview and detailed pictures of Neuro-2a cells, stably transfected with human APP695, are shown. Cells were treated with 0, 10 and 100 μM of Mosd1, respectively. The left panel shows untreated hAPP695-transfected Neuro-2a cells. In the middle and right panel, incubation of hAPP695-transfected Neuro-2a cells with 10 μM Mosd1 and 100 μM Mosd1 are shown. Cell viability and morphology were analyzed with a LSM 710 laser scanning microscope. Scale bars equate 50 μm .

doi:10.1371/journal.pone.0147470.g010

as shown in TEM, AFM and SDS-PAGE studies by several research groups [44, 45]. Additionally, Mosd1 is able to decelerate $\text{A}\beta_{1-42}$ aggregation. Therefore, Mosd1 is able to reduce the impact of already formed $\text{A}\beta_{1-42}$ seeds on monomeric $\text{A}\beta_{1-42}$ and their conversion into toxic aggregates as shown by Seeding ThT Assay.

According to cell culture experiments, aggregates generated by coinubation of $\text{A}\beta_{1-42}$ with Mosd1 are not toxic to PC-12 cells, whereas, the mixture of $\text{A}\beta_{1-42}$ species not treated with Mosd1 showed significant cellular toxicity. Other compounds, which consist of aromates or include aromatic side chains, were also reported to reduce $\text{A}\beta$ induced cell toxicity [43, 45, 46]. This might be contributed to the binding to $\text{A}\beta_{1-42}$ monomers and prevention of their aggregation as well as to the conversion of toxic oligomeric $\text{A}\beta_{1-42}$ species into large non-toxic species as shown in the latter experiments.

Additionally, we were able to show that human APP695 transfected Neuro-2a cells, treated with Mosd1, appear healthier compared to untreated cells, which develop a pathological phenotype. Mosd1 is able to reverse the effects of human APP695 expression and its cleavage products like reduced cell contacts and a lack of cellular protrusions.

Despite the fact that Mosd1 reduces $\text{A}\beta_{1-42}$ toxicity by modulating the equilibrium of $\text{A}\beta_{1-42}$ species, it needs to be assured, that the compound is safe and does not interfere with related but physiological relevant pathways. For example, γ -secretases are involved in the cleavage of APP, leading subsequently to $\text{A}\beta$. Moreover, γ -secretases are also involved in cleavage of transmembrane Notch and therefore interfere with Notch signaling pathways. Alterations within the Notch pathway can lead to severe side effects [47, 48]. According to our results Mosd1 has no effect on γ -secretase activity.

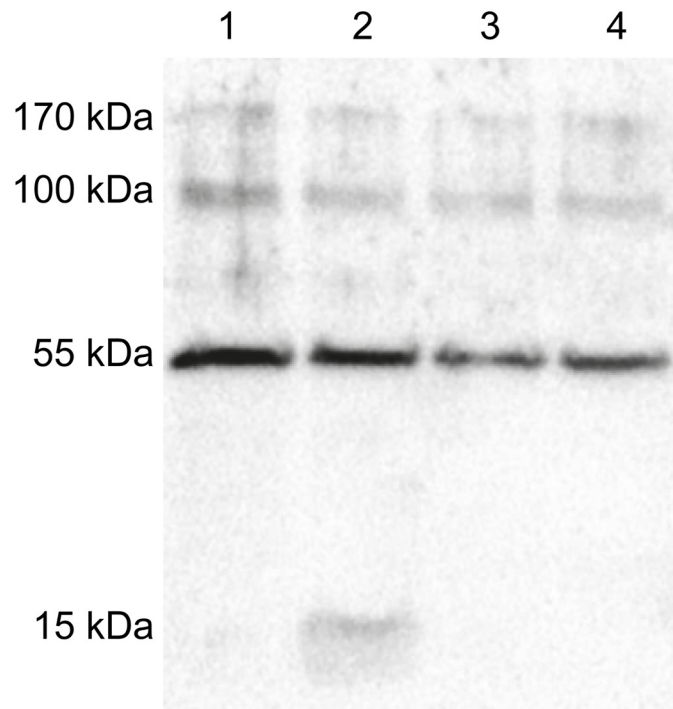


Fig 11. Analysis of potential γ -secretase activity alterations by Mosd1. Detection of CTF β and β -actin by enhanced chemoluminescence on a Western blot of lysed human APP695-transfected Neuro-2a cells. Human APP695-transfected Neuro-2a cells were grown in 24-well plates for 24 hours. Cells were incubated with DMSO (lane 1), DAPT (lane 2), 10 μ M Mosd1 (lane 3) or 100 μ M Mosd1 (lane 4) for additional 24 hours. The cells were harvested, lysed and proteins were separated by Tris-tricine SDS-PAGE. Proteins were blotted on a PVDF membrane and detected with an anti-APP-CTF antibody as well as an anti- β -actin antibody. Binding of HRP conjugated secondary antibodies was detected by transformation of enhanced chemoluminescence (ECL) substrate by HRP.

doi:10.1371/journal.pone.0147470.g011

Given the usefulness of mirror image phage display to obtain stable D-peptides for synthetically available targets, we wonder why there have been only a limited number of reports describing such approaches [49–52] and those described in reviews [26, 34, 53].

Conclusion

Taken together, we have established a novel competitive mirror image phage display for the selection of D-enantiomeric peptides, which bind specifically to monomeric A β_{1-42} . Using non-biotinylated SEC-derived oligomers and DGC-derived HMW aggregates and fibrils of A β_{1-42} as counterselective agents, we were able to enrich phages, which bind specifically to the immobilized biotinylated monomeric A β_{1-42} .

One of our selected D-enantiomeric peptides, Mosd1, shows promising characteristics in several *in vitro* experiments. This leads to the assumption that Mosd1 is able to stabilize A β_{1-42} monomers, interferes with seeded growth and modulates A β_{1-42} aggregation towards non-toxic, amorphous aggregates and therefore rescues cells from A β_{1-42} derived toxicity and reverses pathological phenotypes from hAPP-transfected neuronal cells.

Mosd1 also does not affect γ -secretase function which makes it safer and more precise than γ -secretase modulating compounds. Its small size should facilitate blood-brain-barrier transfer and the D-enantiomeric conformation enables high proteolytic stability. Further investigations

including affinity studies and epitope mapping should provide more information about the mechanism how Mosd1 modulates $A\beta_{1-42}$.

We were able to show that a competitive mirror image phage display is a straightforward method to select compounds, which are $A\beta_{1-42}$ monomer specific and able to modulate $A\beta_{1-42}$ aggregation towards non-toxic species and therefore exhibit high therapeutic potential.

Author Contributions

Conceived and designed the experiments: SR JK SAF DW. Performed the experiments: SR ANK CS MT AE. Analyzed the data: SR JK DW. Contributed reagents/materials/analysis tools: OB CT LG DW. Wrote the paper: SR ANK JK DW.

References

1. Organization WH. Dementia: A Public Health Priority: World Health Organization; 2012.
2. Querfurth HW, LaFerla FM. Alzheimer's disease. *The New England journal of medicine*. 2010; 362(4):329–44. Epub 2010/01/29. doi: [10.1056/NEJMra0909142](https://doi.org/10.1056/NEJMra0909142) PMID: [20107219](https://pubmed.ncbi.nlm.nih.gov/20107219/).
3. Ritchie K, Lovestone S. The dementias. *Lancet*. 2002; 360(9347):1759–66. Epub 2002/12/14. PMID: [12480441](https://pubmed.ncbi.nlm.nih.gov/12480441/).
4. Bauer J. [Clinical diagnosis and therapeutic possibilities for dementia of the Alzheimer type]. *Fortschritte der Neurologie-Psychiatrie*. 1994; 62(11):417–32. Epub 1994/11/01. doi: [10.1055/s-2007-1002299](https://doi.org/10.1055/s-2007-1002299) PMID: [7829030](https://pubmed.ncbi.nlm.nih.gov/7829030/).
5. Selkoe DJ. Translating cell biology into therapeutic advances in Alzheimer's disease. *Nature*. 1999; 399(6738 Suppl):A23–31. Epub 1999/07/07. PMID: [10392577](https://pubmed.ncbi.nlm.nih.gov/10392577/).
6. Thal DR, Rub U, Orantes M, Braak H. Phases of A beta-deposition in the human brain and its relevance for the development of AD. *Neurology*. 2002; 58(12):1791–800. Epub 2002/06/27. PMID: [12084879](https://pubmed.ncbi.nlm.nih.gov/12084879/).
7. Kang J, Lemaire HG, Unterbeck A, Salbaum JM, Masters CL, Grzeschik KH, et al. The precursor of Alzheimer's disease amyloid A4 protein resembles a cell-surface receptor. *Nature*. 1987; 325(6106):733–6. Epub 1987/02/19. doi: [10.1038/325733a0](https://doi.org/10.1038/325733a0) PMID: [2881207](https://pubmed.ncbi.nlm.nih.gov/2881207/).
8. Selkoe DJ, Podlisny MB, Joachim CL, Vickers EA, Lee G, Fritz LC, et al. Beta-amyloid precursor protein of Alzheimer disease occurs as 110- to 135-kilodalton membrane-associated proteins in neural and nonneural tissues. *Proceedings of the National Academy of Sciences of the United States of America*. 1988; 85(19):7341–5. Epub 1988/10/01. PMID: [3140239](https://pubmed.ncbi.nlm.nih.gov/3140239/); PubMed Central PMCID: PMC282182.
9. McLean CA, Cherny RA, Fraser FW, Fuller SJ, Smith MJ, Beyreuther K, et al. Soluble pool of Abeta amyloid as a determinant of severity of neurodegeneration in Alzheimer's disease. *Annals of neurology*. 1999; 46(6):860–6. Epub 1999/12/10. PMID: [10589538](https://pubmed.ncbi.nlm.nih.gov/10589538/).
10. Haass C, Selkoe DJ. Soluble protein oligomers in neurodegeneration: lessons from the Alzheimer's amyloid beta-peptide. *Nature reviews Molecular cell biology*. 2007; 8(2):101–12. Epub 2007/01/25. doi: [10.1038/nrm2101](https://doi.org/10.1038/nrm2101) PMID: [17245412](https://pubmed.ncbi.nlm.nih.gov/17245412/).
11. Cizas P, Budvytyte R, Morkuniene R, Moldovan R, Broccio M, Losche M, et al. Size-dependent neurotoxicity of beta-amyloid oligomers. *Archives of biochemistry and biophysics*. 2010; 496(2):84–92. Epub 2010/02/16. doi: [10.1016/j.abb.2010.02.001](https://doi.org/10.1016/j.abb.2010.02.001) PMID: [20153288](https://pubmed.ncbi.nlm.nih.gov/20153288/); PubMed Central PMCID: PMC2853175.
12. Lambert MP, Barlow AK, Chromy BA, Edwards C, Freed R, Liosatos M, et al. Diffusible, nonfibrillar ligands derived from Abeta1-42 are potent central nervous system neurotoxins. *Proceedings of the National Academy of Sciences of the United States of America*. 1998; 95(11):6448–53. Epub 1998/05/30. PMID: [9600986](https://pubmed.ncbi.nlm.nih.gov/9600986/); PubMed Central PMCID: PMC27787.
13. Zahs KR, Ashe KH. beta-Amyloid oligomers in aging and Alzheimer's disease. *Frontiers in aging neuroscience*. 2013; 5:28. Epub 2013/07/13. doi: [10.3389/fnagi.2013.00028](https://doi.org/10.3389/fnagi.2013.00028) PMID: [23847532](https://pubmed.ncbi.nlm.nih.gov/23847532/); PubMed Central PMCID: PMC3701119.
14. Connelly L, Jang H, Arce FT, Capone R, Kotler SA, Ramachandran S, et al. Atomic force microscopy and MD simulations reveal pore-like structures of all-D-enantiomer of Alzheimer's beta-amyloid peptide: relevance to the ion channel mechanism of AD pathology. *The journal of physical chemistry B*. 2012; 116(5):1728–35. Epub 2012/01/06. doi: [10.1021/jp2108126](https://doi.org/10.1021/jp2108126) PMID: [22217000](https://pubmed.ncbi.nlm.nih.gov/22217000/).
15. Larson ME, Lesne SE. Soluble Abeta oligomer production and toxicity. *Journal of neurochemistry*. 2012; 120 Suppl 1:125–39. Epub 2011/11/30. doi: [10.1111/j.1471-4159.2011.07478.x](https://doi.org/10.1111/j.1471-4159.2011.07478.x) PMID: [22121920](https://pubmed.ncbi.nlm.nih.gov/22121920/); PubMed Central PMCID: PMC3254782.

16. Wilcox KC, Lacor PN, Pitt J, Klein WL. Abeta oligomer-induced synapse degeneration in Alzheimer's disease. *Cellular and molecular neurobiology*. 2011; 31(6):939–48. Epub 2011/05/04. doi: [10.1007/s10571-011-9691-4](https://doi.org/10.1007/s10571-011-9691-4) PMID: [21538118](https://pubmed.ncbi.nlm.nih.gov/21538118/); PubMed Central PMCID: PMC3146579.
17. Finder VH, Glockshuber R. Amyloid-beta aggregation. *Neuro-degenerative diseases*. 2007; 4(1):13–27. Epub 2007/04/13. doi: [10.1159/000100355](https://doi.org/10.1159/000100355) PMID: [17429215](https://pubmed.ncbi.nlm.nih.gov/17429215/).
18. Shankar GM, Li S, Mehta TH, Garcia-Munoz A, Shepardson NE, Smith I, et al. Amyloid-beta protein dimers isolated directly from Alzheimer's brains impair synaptic plasticity and memory. *Nature medicine*. 2008; 14(8):837–42. Epub 2008/06/24. doi: [10.1038/nm1782](https://doi.org/10.1038/nm1782) PMID: [18568035](https://pubmed.ncbi.nlm.nih.gov/18568035/); PubMed Central PMCID: PMC2772133.
19. Jin M, Shepardson N, Yang T, Chen G, Walsh D, Selkoe DJ. Soluble amyloid beta-protein dimers isolated from Alzheimer cortex directly induce Tau hyperphosphorylation and neuritic degeneration. *Proceedings of the National Academy of Sciences of the United States of America*. 2011; 108(14):5819–24. Epub 2011/03/23. doi: [10.1073/pnas.1017033108](https://doi.org/10.1073/pnas.1017033108) PMID: [21421841](https://pubmed.ncbi.nlm.nih.gov/21421841/); PubMed Central PMCID: PMC3078381.
20. Townsend M, Shankar GM, Mehta T, Walsh DM, Selkoe DJ. Effects of secreted oligomers of amyloid beta-protein on hippocampal synaptic plasticity: a potent role for trimers. *The Journal of physiology*. 2006; 572(Pt 2):477–92. Epub 2006/02/14. doi: [10.1113/jphysiol.2005.103754](https://doi.org/10.1113/jphysiol.2005.103754) PMID: [16469784](https://pubmed.ncbi.nlm.nih.gov/16469784/); PubMed Central PMCID: PMC1779683.
21. Lal R, Lin H, Quist AP. Amyloid beta ion channel: 3D structure and relevance to amyloid channel paradigm. *Biochimica et biophysica acta*. 2007; 1768(8):1966–75. Epub 2007/06/08. PMID: [17553456](https://pubmed.ncbi.nlm.nih.gov/17553456/); PubMed Central PMCID: PMC2692960.
22. Paranjape GS, Terrill SE, Gouwens LK, Ruck BM, Nichols MR. Amyloid-beta(1–42) protofibrils formed in modified artificial cerebrospinal fluid bind and activate microglia. *Journal of neuroimmune pharmacology: the official journal of the Society on NeuroImmune Pharmacology*. 2013; 8(1):312–22. Epub 2012/12/18. doi: [10.1007/s11481-012-9424-6](https://doi.org/10.1007/s11481-012-9424-6) PMID: [23242692](https://pubmed.ncbi.nlm.nih.gov/23242692/); PubMed Central PMCID: PMC3587657.
23. Du D, Murray AN, Cohen E, Kim HE, Simkovsky R, Dillin A, et al. A kinetic aggregation assay allowing selective and sensitive amyloid-beta quantification in cells and tissues. *Biochemistry*. 2011; 50(10):1607–17. Epub 2011/01/28. doi: [10.1021/bi1013744](https://doi.org/10.1021/bi1013744) PMID: [21268584](https://pubmed.ncbi.nlm.nih.gov/21268584/); PubMed Central PMCID: PMC3051019.
24. Yin RH, Tan L, Jiang T, Yu JT. Prion-like Mechanisms in Alzheimer's Disease. *Current Alzheimer research*. 2014; 11(8):755–64. Epub 2014/09/13. PMID: [25212914](https://pubmed.ncbi.nlm.nih.gov/25212914/).
25. Schumacher TN, Mayr LM, Minor DL Jr, Milhollen MA, Burgess MW, Kim PS. Identification of D-peptide ligands through mirror-image phage display. *Science*. 1996; 271(5257):1854–7. Epub 1996/03/29. PMID: [8596952](https://pubmed.ncbi.nlm.nih.gov/8596952/).
26. Wiesehan K, Willbold D. Mirror-image phage display: aiming at the mirror. *Chembiochem: a European journal of chemical biology*. 2003; 4(9):811–5. Epub 2003/09/10. doi: [10.1002/cbic.200300570](https://doi.org/10.1002/cbic.200300570) PMID: [12964153](https://pubmed.ncbi.nlm.nih.gov/12964153/).
27. Taylor M, Moore S, Mayes J, Parkin E, Beeg M, Canovi M, et al. Development of a proteolytically stable retro-inverso peptide inhibitor of beta-amyloid oligomerization as a potential novel treatment for Alzheimer's disease. *Biochemistry*. 2010; 49(15):3261–72. Epub 2010/03/17. doi: [10.1021/bi100144m](https://doi.org/10.1021/bi100144m) PMID: [20230062](https://pubmed.ncbi.nlm.nih.gov/20230062/).
28. Sela M, Zisman E. Different roles of D-amino acids in immune phenomena. *FASEB journal: official publication of the Federation of American Societies for Experimental Biology*. 1997; 11(6):449–56. Epub 1997/05/01. PMID: [9194525](https://pubmed.ncbi.nlm.nih.gov/9194525/).
29. Tugyi R, Uray K, Ivan D, Fellingner E, Perkins A, Hudecz F. Partial D-amino acid substitution: Improved enzymatic stability and preserved Ab recognition of a MUC2 epitope peptide. *Proceedings of the National Academy of Sciences of the United States of America*. 2005; 102(2):413–8. Epub 2005/01/05. doi: [10.1073/pnas.0407677102](https://doi.org/10.1073/pnas.0407677102) PMID: [15630090](https://pubmed.ncbi.nlm.nih.gov/15630090/); PubMed Central PMCID: PMC544305.
30. van Groen T, Kadish I, Wiesehan K, Funke SA, Willbold D. In vitro and in vivo staining characteristics of small, fluorescent, Abeta42-binding D-enantiomeric peptides in transgenic AD mouse models. *ChemMedChem*. 2009; 4(2):276–82. Epub 2008/12/17. doi: [10.1002/cmde.200800289](https://doi.org/10.1002/cmde.200800289) PMID: [19072935](https://pubmed.ncbi.nlm.nih.gov/19072935/).
31. Poduslo JF, Curran GL, Kumar A, Frangione B, Soto C. Beta-sheet breaker peptide inhibitor of Alzheimer's amyloidogenesis with increased blood-brain barrier permeability and resistance to proteolytic degradation in plasma. *Journal of neurobiology*. 1999; 39(3):371–82. Epub 1999/06/11. PMID: [10363910](https://pubmed.ncbi.nlm.nih.gov/10363910/).
32. Van Regenmortel MH, Muller S. D-peptides as immunogens and diagnostic reagents. *Current opinion in biotechnology*. 1998; 9(4):377–82. Epub 1998/08/28. PMID: [9720264](https://pubmed.ncbi.nlm.nih.gov/9720264/).
33. van Groen T, Wiesehan K, Funke SA, Kadish I, Nagel-Steger L, Willbold D. Reduction of Alzheimer's disease amyloid plaque load in transgenic mice by D3, A D-enantiomeric peptide identified by mirror

- image phage display. *ChemMedChem*. 2008; 3(12):1848–52. Epub 2008/11/19. doi: [10.1002/cmdc.200800273](https://doi.org/10.1002/cmdc.200800273) PMID: [19016284](https://pubmed.ncbi.nlm.nih.gov/19016284/).
34. Funke SA, Willbold D. Mirror image phage display—a method to generate D-peptide ligands for use in diagnostic or therapeutical applications. *Molecular bioSystems*. 2009; 5(8):783–6. Epub 2009/07/16. doi: [10.1039/b904138a](https://doi.org/10.1039/b904138a) PMID: [19603110](https://pubmed.ncbi.nlm.nih.gov/19603110/).
 35. Hoffmann S, Funke SA, Wiesehan K, Moedder S, Gluck JM, Feuerstein S, et al. Competitively selected protein ligands pay their increase in specificity by a decrease in affinity. *Molecular bioSystems*. 2010; 6(1):126–33. Epub 2009/12/22. doi: [10.1039/b910945e](https://doi.org/10.1039/b910945e) PMID: [20024074](https://pubmed.ncbi.nlm.nih.gov/20024074/).
 36. Johansson AS, Berglind-Dehlin F, Karlsson G, Edwards K, Gellerfors P, Lannfelt L. Physicochemical characterization of the Alzheimer's disease-related peptides A beta 1-42Arctic and A beta 1-42wt. *The FEBS journal*. 2006; 273(12):2618–30. Epub 2006/07/05. doi: [10.1111/j.1742-4658.2006.05263.x](https://doi.org/10.1111/j.1742-4658.2006.05263.x) PMID: [16817891](https://pubmed.ncbi.nlm.nih.gov/16817891/).
 37. Ward RV, Jennings KH, Jepras R, Neville W, Owen DE, Hawkins J, et al. Fractionation and characterization of oligomeric, protofibrillar and fibrillar forms of beta-amyloid peptide. *The Biochemical journal*. 2000; 348 Pt 1:137–44. Epub 2000/05/05. PMID: [10794724](https://pubmed.ncbi.nlm.nih.gov/10794724/); PubMed Central PMCID: [PMC1221046](https://pubmed.ncbi.nlm.nih.gov/pmc/PMC1221046/).
 38. Rzepecki P, Nagel-Steger L, Feuerstein S, Linne U, Molt O, Zadnarc R, et al. Prevention of Alzheimer's disease-associated Abeta aggregation by rationally designed nonpeptidic beta-sheet ligands. *The Journal of biological chemistry*. 2004; 279(46):47497–505. Epub 2004/08/24. doi: [10.1074/jbc.M405914200](https://doi.org/10.1074/jbc.M405914200) PMID: [15322133](https://pubmed.ncbi.nlm.nih.gov/15322133/).
 39. Funke SA, van Groen T, Kadish I, Bartnik D, Nagel-Steger L, Brener O, et al. Oral Treatment with the d-Enantiomeric Peptide D3 Improves the Pathology and Behavior of Alzheimer's Disease Transgenic Mice. *ACS Chemical Neuroscience*. 2010; 1(9):639–48. doi: [10.1021/cn100057j](https://doi.org/10.1021/cn100057j) PMID: [22778851](https://pubmed.ncbi.nlm.nih.gov/22778851/)
 40. Brener O, Dunkelmann T, Gremer L, van Groen T, Mirecka EA, Kadish I, et al. QIAD assay for quantitating a compound's efficacy in elimination of toxic Aβ oligomers. *Scientific Reports*. 2015; 5:13222. doi: [10.1038/srep13222](https://doi.org/10.1038/srep13222) Available: <http://www.nature.com/articles/srep13222#supplementary-information>. PMID: [26394756](https://pubmed.ncbi.nlm.nih.gov/26394756/)
 41. Zettl H, Ness J, Hahnke V, Behr D, Jumpertz T, Saric A, et al. Discovery of gamma-secretase modulators with a novel activity profile by text-based virtual screening. *ACS chemical biology*. 2012; 7(9):1488–95. Epub 2012/06/26. doi: [10.1021/cb3001952](https://doi.org/10.1021/cb3001952) PMID: [22725102](https://pubmed.ncbi.nlm.nih.gov/22725102/).
 42. Sharples RA, Vella LJ, Nisbet RM, Naylor R, Perez K, Barnham KJ, et al. Inhibition of gamma-secretase causes increased secretion of amyloid precursor protein C-terminal fragments in association with exosomes. *FASEB journal: official publication of the Federation of American Societies for Experimental Biology*. 2008; 22(5):1469–78. Epub 2008/01/04. doi: [10.1096/fj.07-9357com](https://doi.org/10.1096/fj.07-9357com) PMID: [18171695](https://pubmed.ncbi.nlm.nih.gov/18171695/).
 43. Ladiwala AR, Dordick JS, Tessier PM. Aromatic small molecules remodel toxic soluble oligomers of amyloid beta through three independent pathways. *The Journal of biological chemistry*. 2011; 286(5):3209–18. Epub 2010/11/26. doi: [10.1074/jbc.M110.173856](https://doi.org/10.1074/jbc.M110.173856) PMID: [21098486](https://pubmed.ncbi.nlm.nih.gov/21098486/); PubMed Central PMCID: [PMC3030325](https://pubmed.ncbi.nlm.nih.gov/pmc/PMC3030325/).
 44. Lu C, Guo Y, Li J, Yao M, Liao Q, Xie Z, et al. Design, synthesis, and evaluation of resveratrol derivatives as Ass((1)-(4)(2)) aggregation inhibitors, antioxidants, and neuroprotective agents. *Bioorganic & medicinal chemistry letters*. 2012; 22(24):7683–7. Epub 2012/11/07. doi: [10.1016/j.bmcl.2012.09.105](https://doi.org/10.1016/j.bmcl.2012.09.105) PMID: [23127891](https://pubmed.ncbi.nlm.nih.gov/23127891/).
 45. Sharoar MG, Thapa A, Shahnawaz M, Ramasamy VS, Woo ER, Shin SY, et al. Keampferol-3-O-rhamnoside abrogates amyloid beta toxicity by modulating monomers and remodeling oligomers and fibrils to non-toxic aggregates. *Journal of biomedical science*. 2012; 19:104. Epub 2012/12/25. doi: [10.1186/1423-0127-19-104](https://doi.org/10.1186/1423-0127-19-104) PMID: [23259691](https://pubmed.ncbi.nlm.nih.gov/23259691/); PubMed Central PMCID: [PMC3541263](https://pubmed.ncbi.nlm.nih.gov/pmc/PMC3541263/).
 46. Chemerovskii-Glikman M, Richman M, Rahimpour S. Structure-based study of anti-amyloidogenic cyclic d,l-α-peptides. *Tetrahedron*. 2014; 70(42):7639–44.
 47. Mikulca JA, Nguyen V, Gajdosik DA, Teklu SG, Giunta EA, Lessa EA, et al. Potential novel targets for Alzheimer pharmacotherapy: II. Update on secretase inhibitors and related approaches. *Journal of clinical pharmacy and therapeutics*. 2014; 39(1):25–37. Epub 2013/12/10. doi: [10.1111/jcpt.12112](https://doi.org/10.1111/jcpt.12112) PMID: [24313554](https://pubmed.ncbi.nlm.nih.gov/24313554/).
 48. Olsauskas-Kuprys R, Zlobin A, Osipo C. Gamma secretase inhibitors of Notch signaling. *OncoTargets and therapy*. 2013; 6:943–55. Epub 2013/08/01. doi: [10.2147/OTT.S33766](https://doi.org/10.2147/OTT.S33766) PMID: [23901284](https://pubmed.ncbi.nlm.nih.gov/23901284/); PubMed Central PMCID: [PMC3726525](https://pubmed.ncbi.nlm.nih.gov/pmc/PMC3726525/).
 49. Welch BD, Francis JN, Redman JS, Paul S, Weinstock MT, Reeves JD, et al. Design of a potent D-peptide HIV-1 entry inhibitor with a strong barrier to resistance. *Journal of virology*. 2010; 84(21):11235–44. Epub 2010/08/20. doi: [10.1128/JVI.01339-10](https://doi.org/10.1128/JVI.01339-10) PMID: [20719956](https://pubmed.ncbi.nlm.nih.gov/20719956/); PubMed Central PMCID: [PMC2953169](https://pubmed.ncbi.nlm.nih.gov/pmc/PMC2953169/).
 50. Chang HN, Liu BY, Qi YK, Zhou Y, Chen YP, Pan KM, et al. Blocking of the PD-1/PD-L1 Interaction by a D-Peptide Antagonist for Cancer Immunotherapy. *Angewandte Chemie*. 2015; 54(40):11760–4. Epub 2015/08/12. doi: [10.1002/anie.201506225](https://doi.org/10.1002/anie.201506225) PMID: [26259671](https://pubmed.ncbi.nlm.nih.gov/26259671/).

51. James TC, Bond U. Molecular mimics of the tumour antigen MUC1. *PloS one*. 2012; 7(11):e49728. Epub 2012/11/21. doi: [10.1371/journal.pone.0049728](https://doi.org/10.1371/journal.pone.0049728) PMID: [23166757](https://pubmed.ncbi.nlm.nih.gov/23166757/); PubMed Central PMCID: PMC3498214.
52. Liu M, Li C, Pazgier M, Li C, Mao Y, Lv Y, et al. D-peptide inhibitors of the p53-MDM2 interaction for targeted molecular therapy of malignant neoplasms. *Proceedings of the National Academy of Sciences of the United States of America*. 2010; 107(32):14321–6. Epub 2010/07/28. doi: [10.1073/pnas.1008930107](https://doi.org/10.1073/pnas.1008930107) PMID: [20660730](https://pubmed.ncbi.nlm.nih.gov/20660730/); PubMed Central PMCID: PMC2922601.
53. Sun N, Funke SA, Willbold D. Mirror image phage display—generating stable therapeutically and diagnostically active peptides with biotechnological means. *Journal of biotechnology*. 2012; 161(2):121–5. Epub 2012/06/26. doi: [10.1016/j.jbiotec.2012.05.019](https://doi.org/10.1016/j.jbiotec.2012.05.019) PMID: [22728425](https://pubmed.ncbi.nlm.nih.gov/22728425/).